© 2015. Published by The Company of Biologists Ltd | Development (2015) 142, 1948-1959 doi:10.1242/dev.119149

RESEARCH ARTICLE

STEM CELLS AND REGENERATION

Generation of sensory hair cells by genetic programming with a combination of transcription factors

Aida Costa[1,*], Luis Sanchez-Guardado[1,2], Stephanie Juniat[3], Jonathan E. Gale[3], Nicolas Daudet[3] and Domingos Henrique[1,2,‡]

ABSTRACT

Mechanosensory hair cells (HCs) are the primary receptors of our senses of hearing and balance. Elucidation of the transcriptional networks regulating HC fate determination and differentiation is crucial not only to understand inner ear development but also to improve cell replacement therapies for hearing disorders. Here, we show that combined expression of the transcription factors Gfi1, Pou4f3 and Atoh1 can induce direct programming towards HC fate, both during *in vitro* mouse embryonic stem cell differentiation and following ectopic expression in chick embryonic otic epithelium. Induced HCs (iHCs) express numerous HC-specific markers and exhibit polarized membrane protrusions reminiscent of stereociliary bundles. Transcriptome profiling confirms the progressive establishment of a HC-specific gene signature during *in vitro* iHC programming. Overall, this work provides a novel approach to achieve robust and highly efficient HC production *in vitro*, which could be used as a model to study HC development and to drive inner ear HC regeneration.

KEY WORDS: Atoh1, Gfi1, Hair cells, Cell type programming, Gene regulation

INTRODUCTION

Sensory hair cells (HCs) of the inner ear are mechanoreceptors that convert the displacements of their specialized apical 'hair' bundle into electrochemical signals. The mammalian inner ear has a very limited capacity to replace lost or damaged HCs (Warchol, 2011), leading to permanent hearing and vestibular impairments for millions of people worldwide. Progress towards understanding the transcriptional networks involved in HC fate specification has led to new strategies for their replacement by gene or stem cell-based therapies. The basic helix-loop-helix (bHLH) transcription factor (TF) Atoh1 has received much attention because it has a key role in HC differentiation. *Atoh1* deletion in mice causes HC loss in all inner ear sensory organs (Bermingham et al., 1999; Cai et al., 2013), whereas its overexpression promotes the generation of ectopic HCs in the developing inner ear (Zheng and Gao, 2000; Woods et al., 2004; Kelly et al., 2012; Liu et al., 2012). However, *Atoh1* is also necessary for the specification of various subsets of neurons (Ben-Arie et al., 1997; Bermingham et al., 2001; Rose et al., 2009), intestinal secretory cells (Yang et al., 2001) and Merkel cells (Maricich et al., 2009), implying that Atoh1 acts in combination with different TFs to activate lineage-specific differentiation programs.

Besides Atoh1, the zinc-finger TF Gfi1 and the POU-domain TF Pou4f3 are the only known transcriptional regulators essential for the proper differentiation and/or survival of all vestibular and auditory HCs (Xiang et al., 1997, 1998; Wallis et al., 2003). The expression of *Gfi1* and *Pou4f3* is initiated in nascent HCs soon after the onset of *Atoh1* upregulation (Wallis et al., 2003; Sage et al., 2006; Pan et al., 2012). These findings raise the hypothesis that Gfi1 and Pou4f3 function together with Atoh1 in determining HC fate in the inner ear.

Previous reports have described relatively complex protocols that are able to steer embryonic stem cell (ESC) differentiation towards HC fate by recapitulating *in vivo* HC development through the temporal control of defined signaling pathways (Oshima et al., 2010; Koehler et al., 2013). Although stepwise differentiation protocols can promote successful HC generation *in vitro*, the efficiency of HC production is relatively low and reproducibility is a potential issue. This limits the use of these methods for inner ear studies in which large cell numbers are needed, such as high-throughput drug screening or cell transplantation therapies. Here, we report a simple, relatively quick and highly efficient protocol to generate sensory HCs *in vitro* from mouse ESCs (mESCs) by simultaneous overexpression of Gfi1, Pou4f3 and Atoh1.

RESULTS

In vitro differentiation of mESCs into HC-like cells

To determine whether Atoh1 or the combination of Gfi1, Pou4f3 and Atoh1 (GPA) can program mESC-derived progenitors into HCs, we first generated two mESC lines (iAtoh1 and iGPA) that enable doxycycline (Dox)-inducible expression of these TFs (Kyba et al., 2002). The iGPA line contains a polycistronic cassette in which Gfi1, Pou4f3 and Atoh1 are linked by 2A peptides (Fig. 1A; supplementary material Fig. S1A,B) to allow robust and balanced co-expression of all three TFs upon Dox addition (supplementary material Fig. S1C-F). In the absence of Dox, no significant expression of the inducible TFs was observed at the mRNA or protein level, whereas Dox treatment led to transgene expression in more than 60% of embryoid body (EB) cells (supplementary material Fig. S1C-F).

We subjected the iAtoh1 and iGPA mESCs to an EB-mediated differentiation protocol in which Dox treatment was initiated at day 4 and maintained during the following 4 days, until day 8, when EBs were collected for analysis (Fig. 1B). Immunostaining for the HC marker Myo7a (El-Amraoui et al., 1996) revealed striking differences between iAtoh1 and iGPA cells. Widespread upregulation of Myo7a was only detected in iGPA-derived EBs (54±2% of cells), and never in EBs derived from iAtoh1 cells, or in

[1]Instituto de Medicina Molecular, Faculdade de Medicina da Universidade de Lisboa, Lisboa 1649-028, Portugal. [2]Champalimaud Neuroscience Programme, Champalimaud Centre for the Unknown, Avenida Brasilia, Lisboa 1400-038, Portugal. [3]UCL Ear Institute, University College London, 332 Gray's Inn Road, London WC1X 8EE, UK.
*Present address: Centre for Integrative Physiology and MRC Centre for Regenerative Medicine, School of Biological Sciences, University of Edinburgh, Edinburgh EH8 9XD, UK.

‡Author for correspondence (henrique@medicina.ulisboa.pt)

Received 19 November 2014; Accepted 15 April 2015

Development (2015) 142, 1948-1959 doi:10.1242/dev.119149

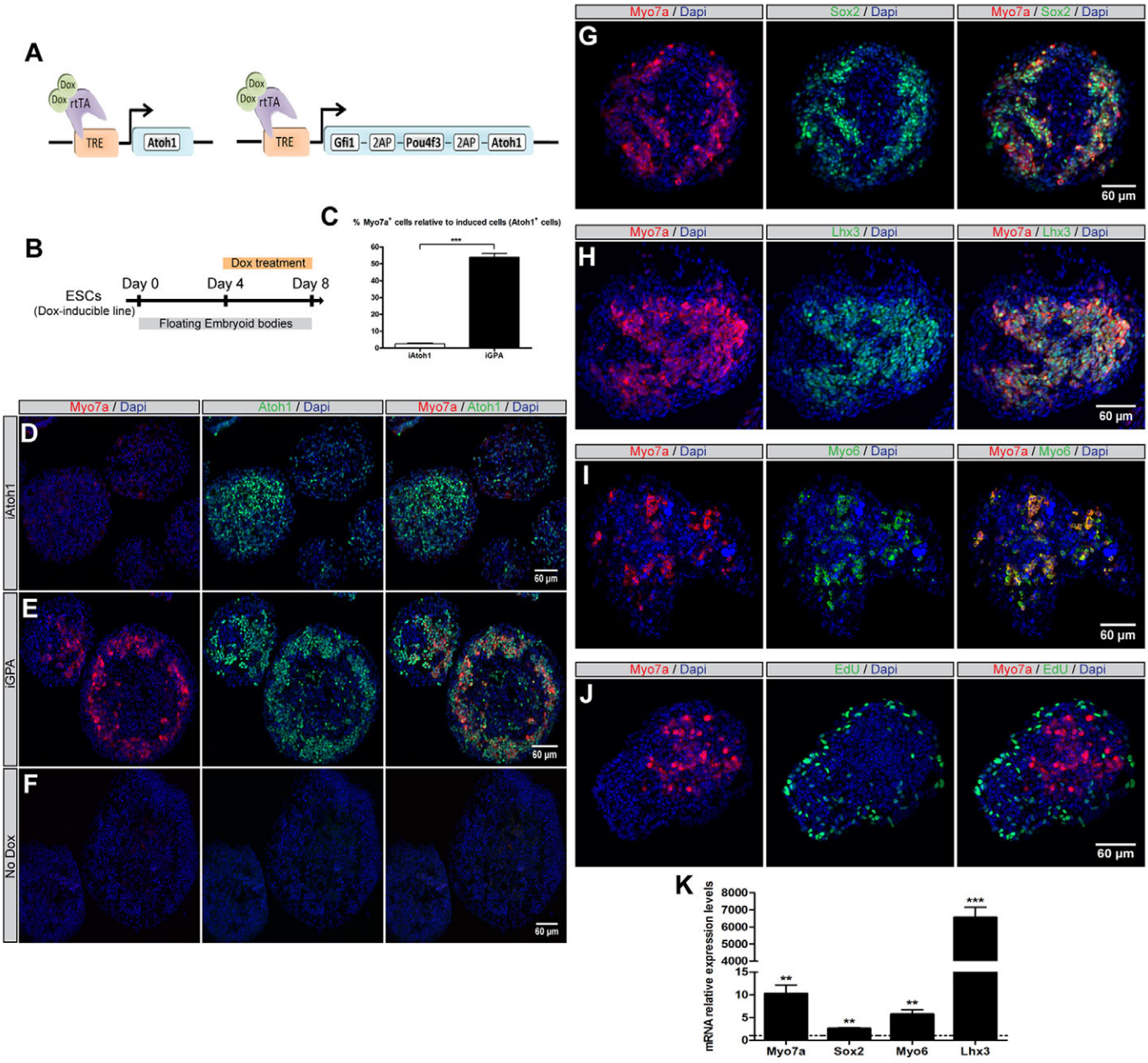

Fig. 1. Inducible expression of Gfi1, Pou4f3 and Atoh1 promotes the differentiation of EB-derived progenitors towards a HC fate. (A) The Dox-inducible iAtoh1 (left) and iGPA (right) lines used in this study. 2AP, 2A peptide; TRE, tetracycline responsive element; rtTA, reverse tetracycline transactivator. (B) mESC differentiation protocol describing the Dox treatment timeline. (C) The mean percentage of Atoh1^{+} cells that are positive for Myo7a in iGPA and iAtoh1 cells after 4 days of Dox treatment. (D-F) Immunostaining analysis of Myo7a and Atoh1 expression in EBs harvested at day 8 from the iAtoh1 (D) and iGPA (E,F) mESC lines. Strong upregulation of Myo7a is detected only in iGPA-derived Atoh1^{+} cells (E). (G-J) Representative images obtained from immunostaining for Myo7a/Sox2 (G), Myo7a/Lhx3 (H), Myo7a/Myo6 (I) and Myo7a/EdU (J) in iGPA EBs, analyzed at day 8 after 4 days of Dox exposure. (K) qRT-PCR analysis reveals upregulation of *Myo7a*, *Sox2*, *Myo6* and *Lhx3* in iGPA-derived EBs treated for 4 days with Dox. Relative expression of each transcript is presented as fold change normalized to the mean of untreated EBs (dotted baseline=1) at day 8. Results are mean±s.e.m. $^{**}P<0.01$, $^{***}P<0.001$ ($n=3$).

the absence of Dox (Fig. 1C-F). This suggests that the combined activities of the three TFs favor commitment towards a HC fate.

To investigate further the identity of induced Myo7a^{+} (iMyo7a^{+}) cells in iGPA-derived EBs, we examined the expression of markers known to be expressed at the onset of vestibular and auditory HC differentiation, such as Sox2, Lhx3 and Myo6 (Xiang et al., 1998; Hume et al., 2007). Notably, all iMyo7a^{+} cells were found to co-express these markers (Fig. 1G-I). Quantitative reverse transcription PCR (qRT-PCR) analyses also confirmed the significant increase in their transcript levels, as compared with untreated EBs (Fig. 1K). By contrast, forced expression of Atoh1 alone in iAtoh1 EBs never resulted in upregulation of HC markers (including Gfi1, Pou4f3 and hair bundle markers) (supplementary material Fig. S2A-F).

We tested whether forced Atoh1 expression might lead to cell death, as implied by Liu et al. (2012). Given the known role of Gfi1 and Pou4f3 in promoting cell survival, their activity might counteract Atoh1 function and contribute to the differences in HC induction between iAtoh1 and iGPA EBs. However, no significant differences were found in the percentage of apoptotic cells between iAtoh1^{+} and iGPA^{+} cells (supplementary material Fig. S3A-D),

Development (2015) 142, 1948-1959 doi:10.1242/dev.119149

indicating that the sustained expression of any of these TFs has no effect on the overall level of cell death in EBs, and that their differing effects in terms of HC induction are unlikely to be secondary to different impacts on cell viability.

During inner ear development, Sox2 expression rapidly declines as HC differentiation progresses (Hume et al., 2007). Thus, the strong Sox2 upregulation that we observed in iMyo7a$^+$ cells suggests that these are at an initial phase of HC commitment. To assess their developmental status further, we next tested whether iMyo7a$^+$ cells are already postmitotic, as sensory progenitors first exit the cell cycle before initiating full differentiation as HCs (Ruben, 1967; Matei, et al., 2005; Chen et al., 2002). A 30 min pulse of 5-ethynyl-2′-deoxyuridine (EdU) incorporation was performed 4 days after initiating Dox treatment in iGPA-derived EBs. Immunodetection revealed a clear lack of colocalization between EdU$^+$ and iMyo7a$^+$ cells, indicating that induced cells have already exited the cell cycle by this stage (Fig. 1J). Altogether, these observations suggest that co-expression of Gfi1, Pou4f3 and Atoh1 induces a rapid conversion of EB cells into postmitotic cells with sensory HC characteristics, which we hereafter refer to as induced HC-like cells, or iHCs.

Previous studies have shown that Gfi1, Pou4f3 and Atoh1 are also expressed during development of the central and peripheral nervous systems (Ninkina et al., 1993; Xiang et al., 1995; Ben-Arie et al., 2000; Wallis et al., 2003) and that each of these TFs is necessary for proper differentiation of multiple neuronal cell types (Ben-Arie et al., 1997; Bermingham et al., 2001; Wang et al., 2002; Tsuda et al., 2005; Rose et al., 2009). We therefore tested whether expression of the three TFs, or of Atoh1 alone, might also promote neuronal differentiation during EB differentiation by examining the expression of neuronal marker Tuj1 (Tubb3) and neural progenitor marker nestin, which are not expressed in mammalian HCs (Malgrange et al., 2002; Wallis et al., 2003). We found that iGPA-derived EBs treated with Dox for 4 days do not exhibit any increase of either Tuj1 or nestin expression (supplementary material Fig. S2G,H). By contrast, iAtoh1-derived EBs show strong Tuj1 expression in most Atoh1-overexpressing cells (supplementary material Fig. S2G). The absence of nestin expression in iAtoh1-derived EBs (supplementary material Fig. S2H) suggests that Atoh1 promotes direct conversion into neurons rather than inducing neural progenitors. These observations are consistent with previous *in vivo* studies showing that Atoh1 overexpression is sufficient to promote neural differentiation in non-neural ectoderm progenitors (Kim et al., 1997). Together, these results indicate that whereas Atoh1 is able to convert EB cells into neurons, the combination of Atoh1, Gfi1 and Pou4f3 drives progression towards a HC fate.

iHC generation is enhanced by retinoic acid or inhibition of Notch signaling

In the embryo, HC differentiation is regulated by the Notch and retinoic acid (RA) signaling pathways, which can be manipulated to cause an increase in HC production: disruption of Notch signaling with gamma-secretase inhibitors leads to the overproduction of HCs at the expense of SCs (Kiernan, 2013), while RA supplementation of cultures of otic vesicles and sensory explants promotes the generation of extra HCs (Represa et al., 1990; Kelley et al., 1993). Hence, we tested whether the efficiency of GPA-induced HC programming could be enhanced in a similar way. We exposed iGPA-derived EBs to 4 days of Dox treatment combined with either the gamma-secretase inhibitor LY411575 or RA (Fig. 2A).

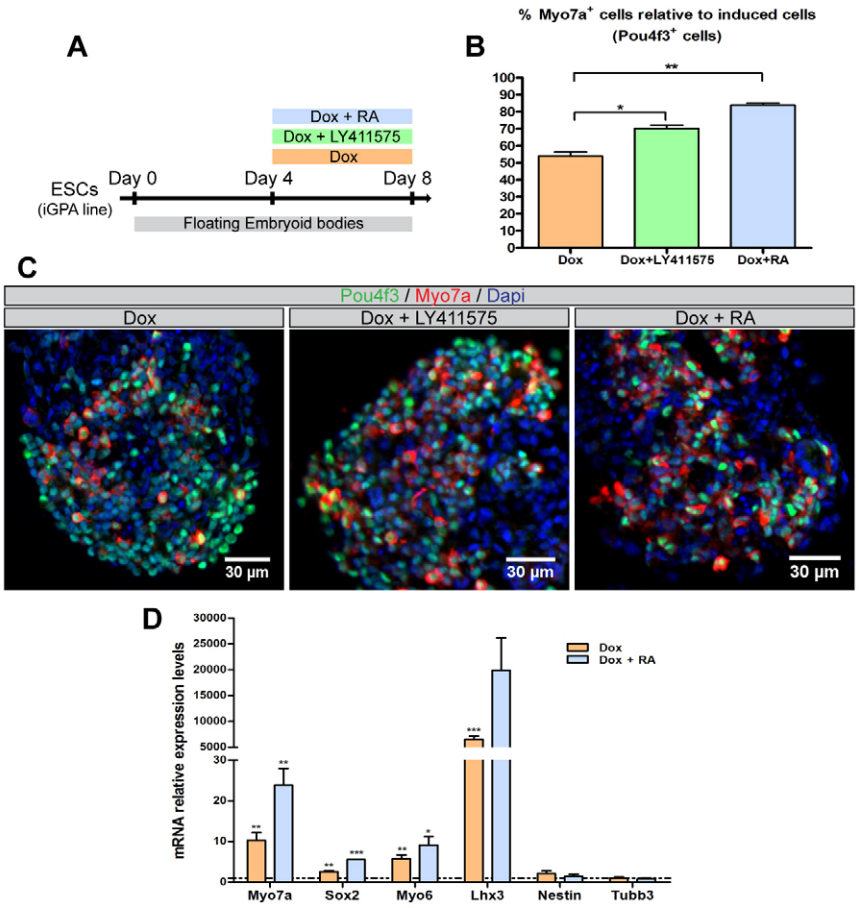

Fig. 2. Enhancing HC programming efficiency by Notch inhibition or RA exposure. (A) iGPA EB differentiation protocols, including the combinatorial treatment with Dox plus LY411575 or RA. (B) Quantification of Myo7a$^+$ cells among cells expressing the three TFs (Pou4f3$^+$ cells) analyzed in 8 day EBs treated with Dox, Dox+LY411575 and Dox+RA. (C) Representative images of iGPA-derived EBs at day 8 obtained by immunostaining of Pou4f3 and Myo7a, showing the significant increase in Myo7a$^+$ cells upon combined treatment with Dox+LY411575 or with Dox+RA, as compared with Dox treatment alone. (D) qRT-PCR analysis shows higher expression levels of HC markers (*Myo7a*, *Sox2*, *Myo6* and *Lhx3*) but not neuronal markers (nestin and *Tubb3*) in EBs treated with Dox+RA, as compared with Dox treatment. Fold change was normalized to the mean of untreated EBs (dotted baseline=1). Results are mean±s.e.m. **P*<0.05, ***P*<0.01, ****P*<0.001 (*n*=3).

Development (2015) 142, 1948-1959 doi:10.1242/dev.119149

Remarkably, the proportion of iHCs increased significantly in the presence of LY411575 (70±2%) or RA (84±1%) when compared with the Dox treatment alone (54±2%) (Fig. 2B,C). In addition, mRNA expression levels of *Myo7a*, *Sox2*, *Myo6* and *Lhx3* were significantly elevated by RA treatment of iGPA EBs (Fig. 2D), confirming that RA enhances HC programming efficiency. We also examined the expression of nestin and *Tubb3*, as neuronal commitment can occur upon RA treatment in differentiating EBs (Li et al., 1998). However, no significant upregulation of either of these neural markers was detected (Fig. 2D), suggesting that the effect of RA on HC differentiation is specific.

iHCs are able to develop hair bundle-like structures

To determine whether iHCs are capable of developing stereociliary bundles similar to those of sensory HCs *in vivo*, we examined the expression of espin, one of the major actin-bundling proteins of stereocilia (Zheng et al., 2000b), in iGPA-derived EBs (Fig. 3A-C′). Immunostaining revealed weak espin expression within GPA-expressing cells at day 8, after 4 days of Dox treatment (Fig. 3B). However, it is known that the onset of espin expression during normal inner ear development occurs later than that of Myo7a (Chen et al., 2002; Sekerkova et al., 2006), raising the possibility that day 8 iHCs were still at an initial stage of HC differentiation. We therefore extended the period of Dox treatment for an additional 4 days and examined EBs at day 12 (Fig. 3C). Notably, at this later time point, high levels of espin are present in polarized membrane projections emanating from iHCs (Fig. 3C). These espin-rich protrusions were observed in 55±3% of Myo7a$^+$ cells, a percentage that was not increased by RA treatment (55±6%). Another essential hair bundle protein, cadherin 23 (Cdh23) (Siemens et al., 2004), was also detected in the iHC protrusions at day 12 (supplementary material Fig. S4A). A significant increase in the expression of *Espn* and *Cdh23* at day 12 compared with day 8 was also found by qRT-PCR (Fig. 3D). The concurrent decline of Sox2 levels in iHCs between day 8 and day 12 (Fig. 3D; supplementary material Fig. S4C) further supports the idea that iHCs progress towards a more mature HC phenotype (Fritzsch et al., 2015).

We noted that the espin-rich protrusions in iHCs show heterogeneous morphology and, although apparently polarized, do not exhibit consistent orientation (Fig. 3C′). We hypothesized that exposing iHCs to inner ear polarity cues might improve the morphological differentiation of their hair bundle-like structures (Oshima et al., 2010). To test this idea, we established a co-culture system in which iGPA-derived EBs were dissociated and plated on the surface of mitotically inactivated utricle mesenchymal cells for 6 days, in the presence of Dox and RA (Fig. 3E). Although we did not observe a clear epithelial organization with defined polarity among iHCs in these co-cultures, detailed confocal analysis revealed that the espin-rich projections are preferentially directed towards either the bottom or the top of the cell layer (Fig. 3F-I; supplementary material Fig. S4B). In addition, actin filaments were also present in these espin-rich protrusions (Fig. 3J), resembling normal HC stereocilia that contain a core of uniformly spaced actin filaments cross-linked with espin.

In agreement with the immunostaining data, scanning electron microscopy (SEM) showed that elongated membrane protrusions reminiscent of hair bundles are present at the apical surface of some iHCs (Fig. 3K). However, the vast majority of these putative bundles are poorly organized compared with normal HC stereociliary bundles, indicating that the maturation of hair bundle-like structures in iHCs is incomplete under these culture conditions.

Combined expression of Gfi1, Pou4f3 and Atoh1 can induce HC specification and differentiation *in vivo*

The lack of proper hair bundle maturation in iHCs could be due to inappropriate culture conditions, but it might also result from incomplete implementation of a HC differentiation program by Gfi1, Pou4f3 and Atoh1. To address this question, we tested the effects of combined GPA expression *in vivo*, in the developing inner ear of chicken embryos, using a Tet-on inducible Tol2 transposon system that allows spatial and temporal control of transgene expression (Takahashi et al., 2008; Freeman et al., 2012). The otic cup was co-electroporated *in ovo* at E2 with the TRE:GPA-eGFP vector [which contains a bidirectional tetracycline-responsive element (TRE) that drives the expression of both Gfi1-Pou3f4-Atoh1 and eGFP upon Dox treatment] and plasmids encoding the rtTA-M2 Tet-on activator and Tol2 transposase (Fig. 4A). Two days later, the embryos were treated with Dox and incubated for a further 2-4 days, until analysis at E6 or E8 (Fig. 4B). The results show that the combined activity of Gfi1, Pou4f3 and Atoh1 induces Myo7a expression in electroporated cells located in various regions of the developing inner ear (n=14/14 embryos, Fig. 4C,D), including both sensory and non-sensory domains of the vestibular and auditory system. Ectopic Myo7a$^+$ cells could even be found in the epithelium of the endolymphatic duct (a non-sensory component of the endolymphatic system, Fig. 4F).

Among eGFP$^+$ cells analyzed at E6 in the vestibular and auditory regions, 77±2% (n=265) and 76±6% (n=492) showed Myo7a expression, respectively (four independent inner ear samples were analyzed at E6). These ectopic Myo7a$^+$ cells are preferentially located close to the luminal surface of the otic epithelium where HCs normally reside, and express other HC markers such as Sox2, Myo6, hair cell antigen (HCA), otoferlin (HCS-1) and parvalbumin (Fig. 4E-K). They are also correctly polarized, with HCA-positive stereociliary bundles at the luminal surface (Fig. 4H′,I). The production of HCs is delayed in the auditory epithelium compared with the vestibular organs, and HC markers such as Myo7a, Myo6, HCA and HCS-1 are not yet detected in the basilar papilla at E6 (data not shown). Nonetheless, ectopic eGFP$^+$ iHCs located in the sensory and non-sensory regions of the cochlear duct express these HC markers already at E6 (Fig. 4H-J), suggesting that GPA expression can induce rapid commitment towards HC fate independently of the developmental stage and character of the transfected cells. Remarkably, Tuj1$^+$ nerve fibers originating from the otic ganglia appear to be recruited by ectopic eGFP$^+$ HCs at E8, even when these cells are present in non-sensory epithelia (n=3/5, Fig. 4L).

Altogether, these data show that GPA expression can efficiently induce the generation of differentiated HCs from various types of otic progenitors *in vivo*.

Transcriptional profiling of iHCs reveals a specific HC signature

What is the precise genetic program induced by the combined activities of Gfi1, Pou4f3 and Atoh1, and to what extent does it match the transcriptional signature of an HC? To answer these questions, we first sought to obtain homogeneous populations of iHCs for transcriptional profiling. A novel iGPA-derived mESC line was prepared that contains a *Myo7a* promoter-driven fluorescence reporter system to specifically label iHCs. This was based on an established *Myo7a* promoter that, along with a strong HC-specific enhancer located in intron 1 of *Myo7a*, has been shown to drive specific transgene expression in vestibular and auditory HCs (Boeda et al., 2001).

Development (2015) 142, 1948-1959 doi:10.1242/dev.119149

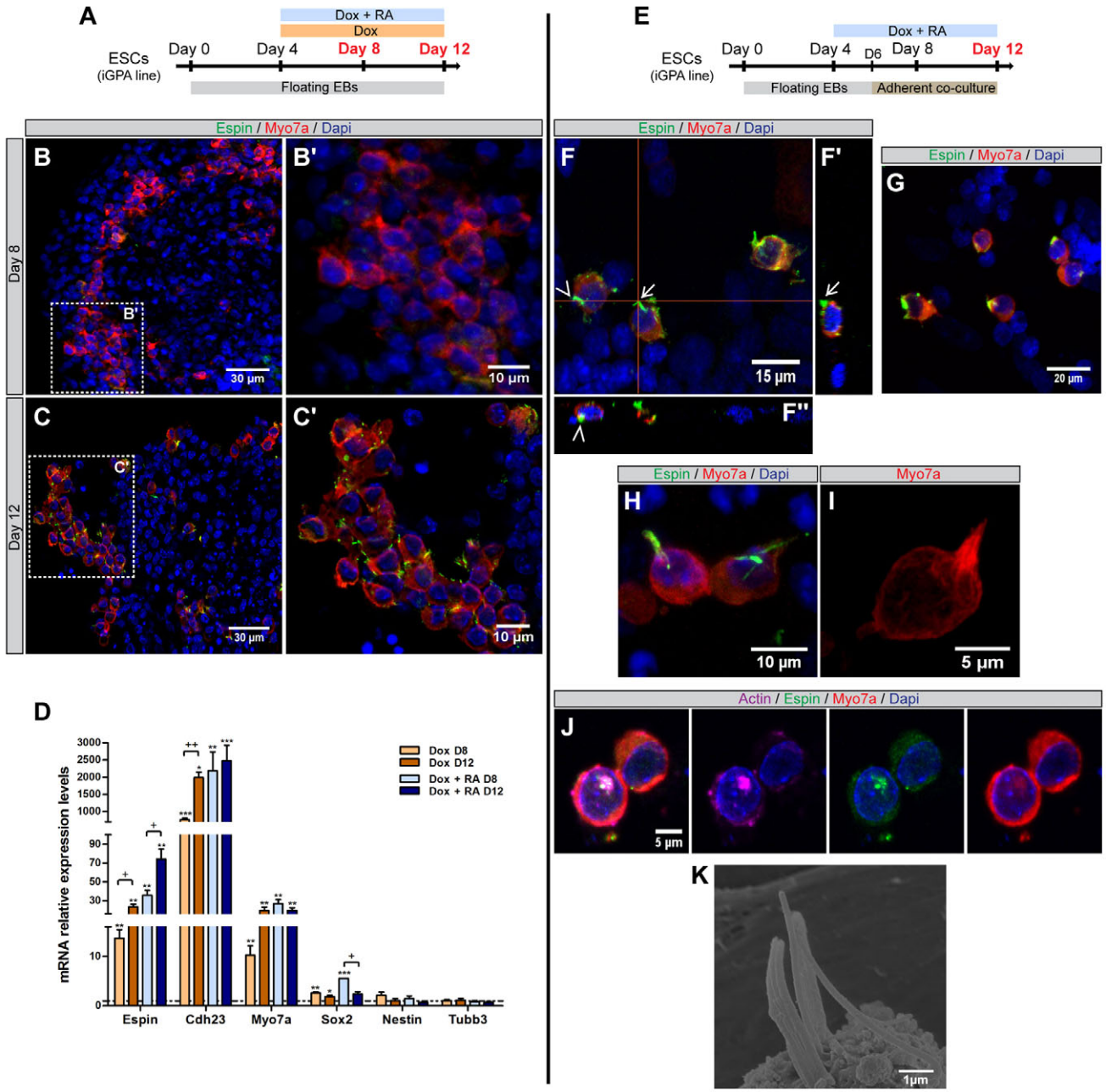

Fig. 3. Morphological characterization of hair bundle-like structures in iHCs. (A) iGPA EB differentiation protocol describing the Dox treatment timeline. (B,C) Immunostaining for espin and Myo7a in iGPA-derived EBs treated with Dox for 4 (B) or 8 (C) days reveals a strong and polarized espin^{+} structure on the surface of iMyo7a^{+} cells. These structures were absent in EBs exposed to Dox for only 4 days (B). (B′,C′) The boxed regions at high magnification. (D) The relative mRNA levels (presented as fold change normalized to the mean of untreated EBs at the corresponding time point; dotted baseline=1) of genes encoding hair bundle markers (*Espn* and *Cdh23*), HC markers (*Myo7a* and *Sox2*) and neuronal markers (nestin and *Tubb3*) in EBs treated with Dox or Dox+RA at day 8 and at day 12. (E) Dissociated EB co-culture differentiation protocol with mitotically inactivated chicken utricle periodic mesenchyme cells. (F) Confocal stacks of hair bundle-like protrusions labeled for Myo7a and espin in the adherent co-cultures at day 12. (F′,F″) Orthogonal views showing espin^{+} structures oriented towards the utricle mesenchyme layer (arrow in F′) or in the opposite direction facing the cell surface (arrowhead in F″). (G-J) Confocal images showing representative espin^{+} and Myo7a^{+} protrusions in several iHCs grown in adherent co-cultures at day 12. Phalloidin immunostaining shows that polarized Myo7a^{+}/espin^{+} structures are F-actin-filled membrane protrusions (J). (K) Morphology of microvilli-like stereocilia protruding from the cell surface of an iHC, as observed by SEM. Results are mean±s.e.m. $^{+}$, $^{*}P$<0.05, $^{++}$, $^{**}P$<0.01, $^{***}P$<0.001 (n=3).

The new inducible reporter mESC line (iGPA-Myo7a:mVenus, Fig. 5A) showed comparable HC programming efficiency and RA sensitivity to the parental iGPA line (Fig. 5B). Although the Myo7a reporter exhibited weak activity in the absence of induction (Fig. 5B, C,E), addition of Dox and RA led not only to a strong increase in the total number of Venus^{+} cells, but also to much higher fluorescence levels per cell (Fig. 5B-D,F). Furthermore, a high degree of correlation between Venus and Myo7a expression was observed in these EBs by immunostaining or by flow cytometry analysis following intracellular antibody staining (Fig. 5F). These results indicate that the Myo7a:mVenus reporter provides an effective readout for *Myo7a* induction during HC programming.

We next used the iGPA-Myo7a:mVenus reporter line and FACS to isolate day 8 and day 12 iHCs from EBs that were treated with either

Development (2015) 142, 1948-1959 doi:10.1242/dev.119149

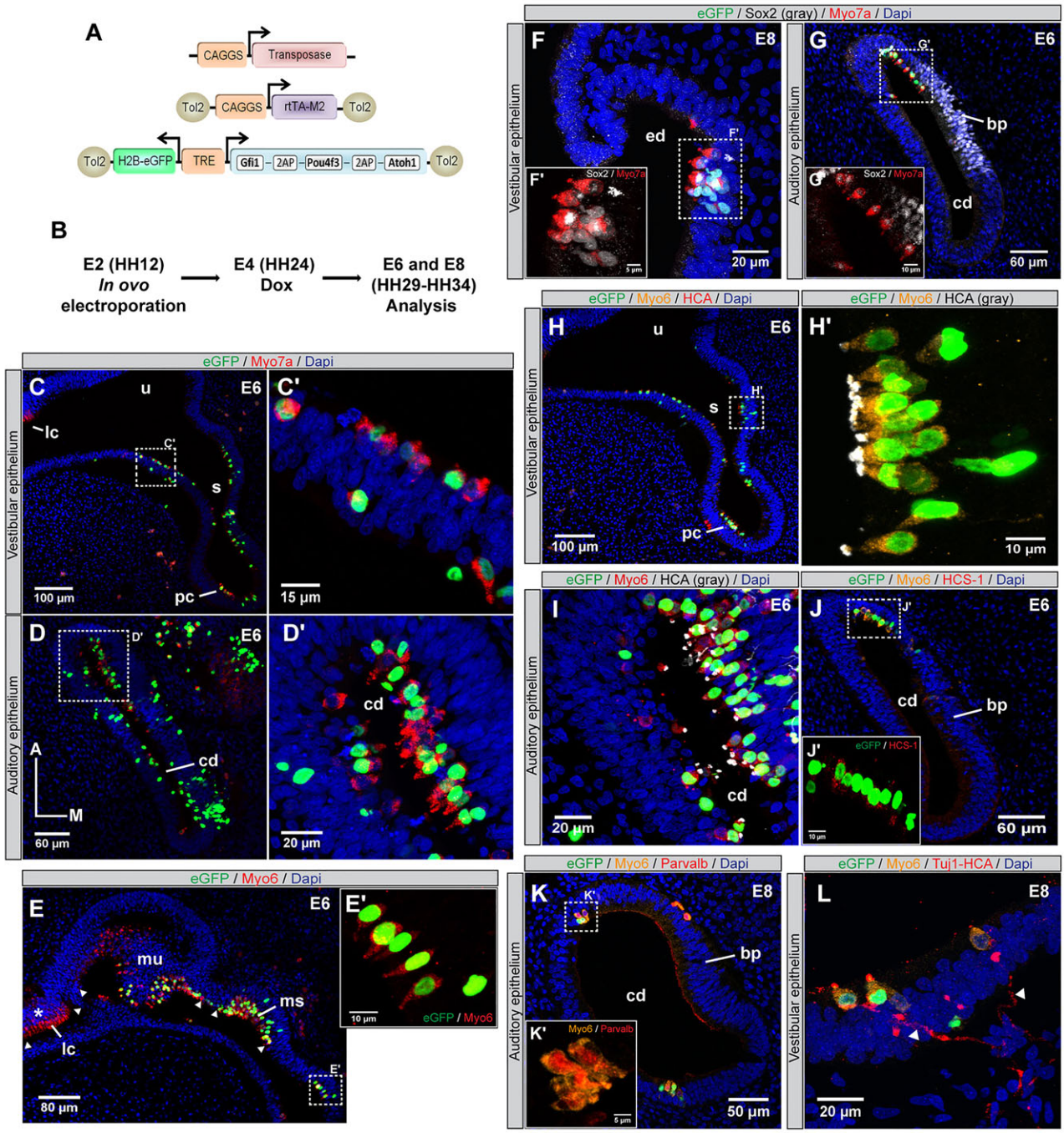

Fig. 4. Induction of Gfi1, Pou4f3 and Atoh1 expression induces HC differentiation in various regions of the embryonic chick inner ear. (A) Expression vectors used for Dox-inducible Gfi1-Pou4f3-Atoh1 and eGFP expression by *in ovo* electroporation. Note that eGFP is fused with histone 2B (H2B) for nuclear localization. (B) Experimental design to test the effects of Gfi1-Pou4f3-Atoh1 expression during inner ear development in the chick embryo. (C,D) Representative images of the vestibular (C) and auditory (D) epithelia showing Myo7a and eGFP immunofluorescence in E6 electroporated embryos. (C′,D′) The boxed regions at high magnification. (E) A section through the vestibular region shows electroporated eGFP^{+} cells with Myo6 expression in various sensory patches (arrowheads), as well as in non-sensory domains of the otic epithelium (E′). Non-electroporated patches with Myo6-expressing HCs are also present (asterisk). (F,G) Immunostaining analysis for Myo7a/eGFP/Sox2 showing expression of Sox2 in ectopic Myo7a^{+} cells (F′,G′). (H,I) Immunostaining analysis for Myo6/eGFP/HCA in the vestibular (H) and auditory (I) epithelium shows polarized localization of HCA in the apical domain of ectopic iHCs (red in H, white in I,H′). (J,K) Analysis of electroporated eGFP^{+} cells in the basilar papilla epithelium shows that ectopic iHCs express the HC markers HCS-1 (J) and parvalbumin (K). (L) Ectopic iHCs (expressing Myo6 and HCA) are innervated by Tuj1-positive neuronal extensions (arrowheads) that project from neurons at the otic ganglion. Some ectopic HCs are eGFP negative, possibly owing to eGFP decay at E8 (Dox was added only at E4). bp, basilar papilla; cd, cochlear duct; lc, lateral crista; u, utriculi; s, sacculi; pc, posterior crista; mu, macula utriculi; ms, macula sacculi; ed, endolymphatic duct. A, anterior; M, medial.

Dox alone or with Dox and RA. Unsorted EBs from the same reporter line, grown in the same conditions but without Dox or RA treatment, were used as controls. Independent RNA preparations from each of the selected time points and treatments (three biological replicates for Dox or Dox+RA treatments, two for 'no treatment') were processed and hybridized on Affymetrix whole-transcript microarrays.

Development (2015) 142, 1948-1959 doi:10.1242/dev.119149

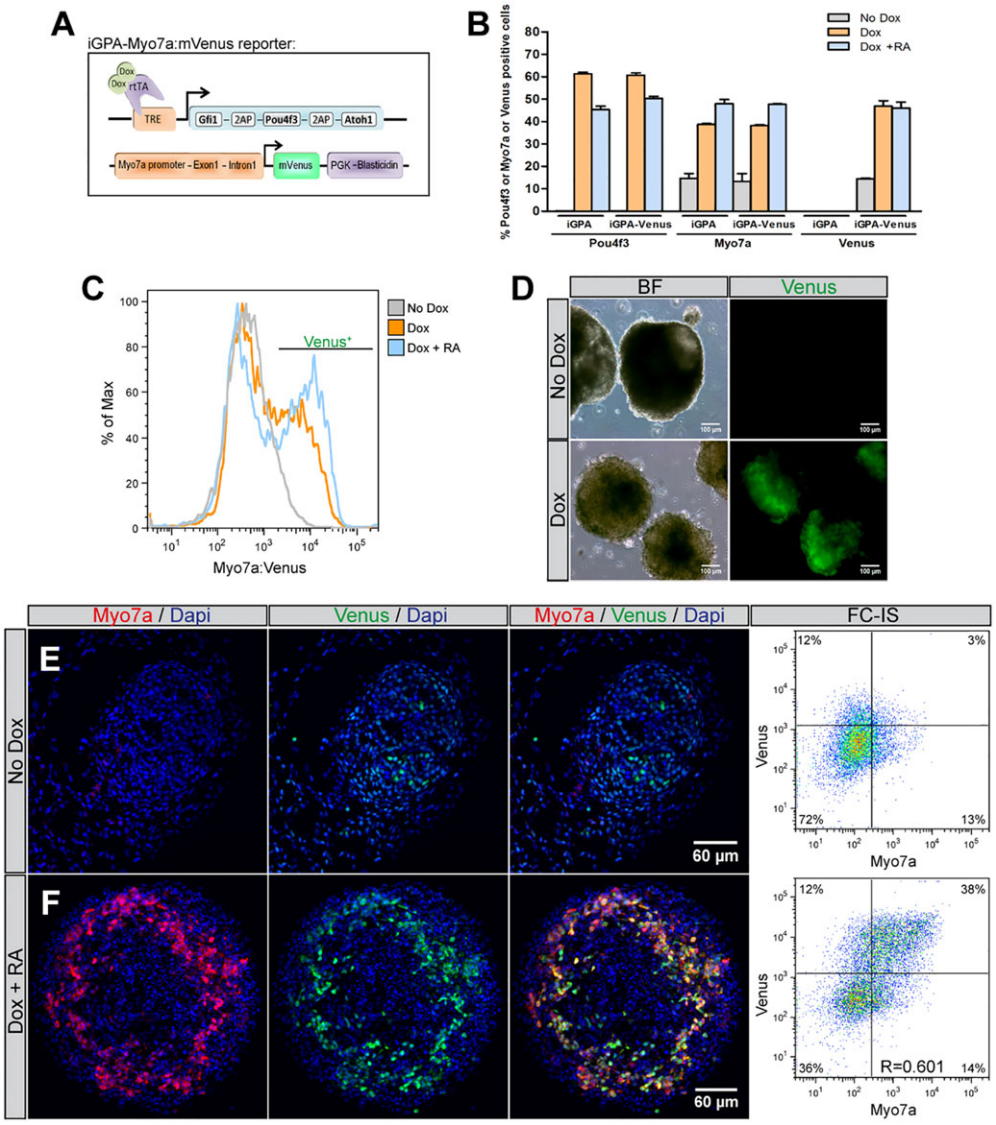

Fig. 5. The iGPA-Myo7a:mVenus ESC line is an adequate fluorescence reporter for Myo7a expression. (A) The iGPA-Myo7a:mVenus ESC line containing the mouse *Myo7a* regulatory regions driving transcription of a Venus fluorescent protein, followed by a selection cassette. PGK, phosphoglycerate kinase promoter; Blasticidin, blasticidin resistance gene. (B) Quantification of Pou4f3^{+}, Myo7a^{+} and Venus^{+} cells relative to total cell numbers found within EBs grown in the absence or presence of Dox and Dox+RA at day 8. Cell counts were performed for EBs generated from the iGPA and iGPA:Myo7a:mVenus lines. No significant differences were found between these two lines regarding the mean percentage of total Pou4f3^{+} and Myo7a^{+} cells in the different treatments. (C) Representative histogram showing Venus expression in iGPA:Myo7a:mVenus-derived EBs that were untreated (14.5±0.4%), treated with Dox (46.9±4.1%) or Dox+RA (46±4.6%) at day 8. (D) Brightfield and fluorescence images of live floating iGPA:Myo7a:mVenus-derived EBs at day 8, showing weak Venus fluorescence levels in the absence of Dox, but high numbers of strongly fluorescent Venus^{+} cells following Dox induction. (E,F) Immunostaining analysis for Myo7a and Venus in iGPA-Myo7a:mVenus-derived EBs, in untreated (E) or Dox+RA conditions (F) at day 8, showing a high degree of colocalization between the two proteins (79.5±0.3% and 54.4±1.7% of Venus^{+} cells were Myo7a^{+} in EBs treated with Dox+RA and Dox, respectively). Included are representative dot plots of intracellular staining for Myo7a and Venus proteins, as analyzed by flow cytometry (FC-IS, flow cytometry analysis following intracellular staining). Statistical analysis indicates a good correlation between the expression of both proteins (Pearson correlation=0.6). Results are mean±s.e.m. (*n*=3).

Hierarchical clustering of the transcriptome datasets revealed a clear segregation between ‘no Dox’ and ‘Dox’ samples (Fig. 6A). Interestingly, in the Dox branch, samples cluster in two groups: one containing day 8 iHCs treated with Dox, and the other composed of day 8 iHCs treated with Dox+RA, together with all the day 12 iHC samples (Fig. 6A). This suggests that day 8 iHCs treated with RA reach a differentiation stage similar to that of day 12 iHCs, indicating that RA treatment improves the efficiency of iHC programming by accelerating the initial differentiation steps. This would be consistent with the earlier onset of Myo7a expression in RA-treated iGPA EBs (supplementary material Fig. S5A-C).

We next analyzed the genes that were differentially expressed in iHC populations obtained with different treatments by comparison with control (‘no Dox’) cells at the same time point (supplementary material Table S1). Genes upregulated in day 8 iHCs were enriched in gene ontology (GO) functional groups related to neuronal differentiation and inner ear development (Fig. 6B,C). The set of upregulated genes in day 12 iHCs was highly enriched in genes involved in inner ear development and HC functions, such as sensory perception of sound/mechanical stimulus and synaptic transmission (Fig. 6D,E). Strikingly, analysis of the subset of day 8 upregulated genes that are further upregulated at day 12 revealed a

Development (2015) 142, 1948-1959 doi:10.1242/dev.119149

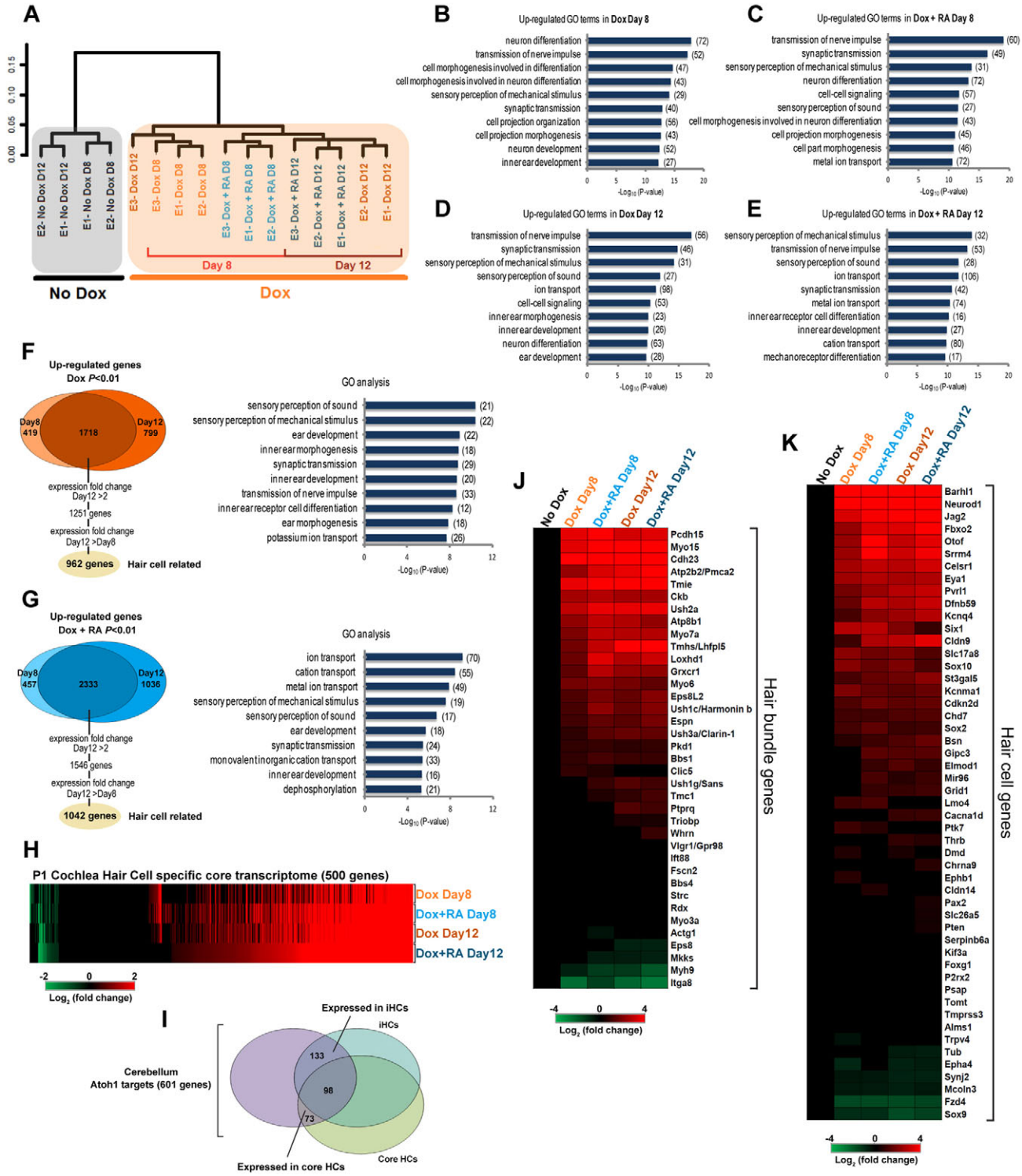

Fig. 6. Analyses of iHC transcriptome profiles. (A) Dendrogram showing hierarchical clustering of the various expression profiles obtained from iGPA-Myo7a:mVenus reporter-derived EBs (E1, E2 and E3 correspond to three biological replicates). (B-E) Gene ontology analysis performed using the DAVID functional annotation tool for genes significantly upregulated (fold change >2, $P<0.01$) in the four iMyo7a:Venus groups relative to uninduced cells. The number of upregulated genes included within each GO functional term is shown. (F,G) Venn diagram illustrating the overlap between the significantly upregulated genes identified in iMyo7a^{+} cells at day 8 and day 12, as compared with uninduced cells. From the list of common upregulated genes in iGPA cells treated with Dox only, those that showed higher fold change at day 12 were selected. This list was subjected to a GO analysis using DAVID. (G) The same procedure was performed for the overlapping genes from iGPA cells cultured with Dox+RA. (H) Heat map depicting the relative fold changes in expression of 500 core HC genes (Cai et al., 2015) across the four iMyo7a groups, relative to uninduced cells ($P<0.05$). (I) Venn diagram illustrating the overlap between the transcriptome of the cochlear core HC signature and of iHCs ($P<0.05$) relative to the 601 cerebellum Atoh1 direct target genes previously identified by Klisch et al. (2011). (J,K) Heat maps depicting the relative fold changes in expression of hair bundle (J) or HC (K) deafness-related genes across the four iMyo7a groups, relative to uninduced cells ($P<0.05$).

Development (2015) 142, 1948-1959 doi:10.1242/dev.119149

stronger enrichment in gene categories involved in HC functions (Fig. 6F,G). Furthermore, GO analysis showed that genes connected to the cell cycle and cell division are specifically repressed in iHCs (supplementary material Fig. S6A-D), consistent with the observation that these cells have ceased proliferation and exited the cell cycle. Altogether, this analysis indicates that the combined activity of Gfi1, Pou4f3 and Atoh1 is able to induce a bona fide HC developmental program. This conclusion is also supported by the significant overlap between the transcriptional profiles of iHCs and Atoh1-GFP-sorted HC populations from P1 mouse cochleas: out of a core HC signature of 500 genes defined for Atoh1-GFP HCs (Cai et al., 2015), 69% are upregulated in iHCs (Fig. 6H). By contrast, only 38% of the defined Atoh1 gene targets in cerebellar granule neuron precursors (CGPs) (Klisch et al., 2011) are upregulated in iHCs (Fig. 6I).

Finally, we analyzed the transcriptome datasets for the expression of genes known to be functionally relevant for inner ear HC development/function. We first selected a list of 250 genes associated with hereditary forms of deafness in mouse or human (http://hearingimpairment.jax.org/master_table1.html), and further refined this gene set by selecting those that are known to be expressed in HCs (supplementary material Table S1, 88 genes). Analysis of their expression in iHCs at different stages showed that the majority of these 88 genes are significantly upregulated by the combined activity of the three TFs, in particular in day 12 iHCs, which exhibit a clear enrichment in expression of deafness genes known to participate in the formation of hair bundles (Fig. 6J,K).

Since multiple genes involved in the mechanoreception machinery are expressed in iHCs, we examined whether functional mechanotransduction channels are also present in these cells by performing an FM1-43 permeation assay (Gale et al., 2001). When co-cultures grown in the absence of Dox were exposed (for 60 s) to FM1-43, no labeled live cells were detected (supplementary material Fig. S7A). By contrast, in Dox-treated cells (day 12 with RA), ~25% of the Venus$^+$ population was labeled by FM1-43 (supplementary material Fig. S7B). The specific internalization of FM1-43 into Venus$^+$ cells suggests that they contain open and potentially functional mechanotransduction channels.

DISCUSSION

We report here that a combination of three TFs (Gfi1, Pou4f3 and Atoh1) is able to promote the direct conversion of somatic cells into HC-like cells, both *in vitro* and *in vivo*. Transcriptome profiling of iHCs at different stages reveals that a specific HC genetic program is activated in these cells. This program appears to recapitulate the normal progression of HC development: genes that are induced early (day 8) are known to participate in HC commitment, while genes encoding components of the mechanotransduction machinery are activated at a later stage of the process (day 12), coinciding with the appearance of polarized espin-rich hair bundle-like protrusions in iHCs. Although these bundles are less organized than native stereociliary bundles, some iHCs are able to rapidly incorporate the FMI-43 dye, which would be consistent with the presence of functional mechanoreceptor channels in these cells. Altogether, our data suggest that Gfi1, Pou4f3 and Atoh1 can activate the genetic program required for the specification and differentiation of functional HCs. However, complete maturation of iHCs is likely to be dependent on additional extrinsic and intrinsic cues.

Combinatorial transcriptional control of HC formation

Our results show that Gfi1, Pou4f3 and Atoh1 are core TFs of the genetic network regulating HC differentiation. Although *Atoh1* has been considered a 'master' gene for HC differentiation owing to its capacity to induce new HCs following ectopic expression in the inner ear (Zheng and Gao, 2000; Woods et al., 2004), our work shows that this pro-HC function is context dependent, as Atoh1 is unable to induce a HC fate in EB cells, driving instead a neuronal differentiation program. By contrast, we show here that the combination of Atoh1 with Gfi1 and Pou4f3 leads to the implementation of a HC differentiation program in EB cells, as well as in non-sensory otic epithelia. These findings unveil a novel regulatory layer in HC fate specification and provide a molecular basis to explain how Atoh1 can induce different cell fates in the embryo – not only HCs in the inner ear, but also Merkel cells in the skin, secretory cells in the intestine, or granule neurons in the cerebellum (Mulvaney and Dabdoub, 2012).

What roles do Gfi1 and Pou4f3 play in this process? Gfi1 is a known transcriptional repressor and previous studies indicate that it might contribute to diverting Atoh1-expressing cells from an exclusively neural differentiation program. For instance, HCs in the inner ear of *Gfi1* mutant mice exhibit abnormal Tuj1 expression, suggesting a partial transformation into neurons (Wallis et al., 2003). Also, in the intestinal epithelium of *Gfi1* null mice, Atoh1-dependent mucous and Paneth cells acquire abnormal Ngn3 expression and can convert to pro-enteroendocrine lineages (Bjerknes and Cheng, 2010). However, Gfi1 may also act as a transcriptional coactivator to positively modulate Atoh1 activity, by analogy with the functional interaction between their *Drosophila* homologs (Senseless and Atonal) during sensory precursor specification (Jarman and Groves, 2013). In this process, Senseless may function to increase or modify the E-box binding specificity of Atonal, modulating its proneural functions. Whether Senseless/Gfi1 acts by direct physical interaction with Atonal/Atoh1, or by binding promoter regions adjacent to E-boxes to modulate Atonal/Atoh1 transcriptional activity, remains to be investigated. However, in the case of HC induction discussed here, it is unlikely that the observed specificity can be ascribed only to the modulatory activity of Gfi1, as the Atoh1/Gfi1 pair is also active during other cell fate decision processes, such as the determination of secretory cell identities in intestinal crypts (Shroyer et al., 2005; Bjerknes and Cheng, 2010).

Although we have not tested whether Pou4f3 is absolutely required for HC induction in EBs, it is likely that this TF also plays an essential role in the process, not only by independently activating an additional set of HC differentiation genes, but also by modulating Atoh1/Gfi1 activity to establish a specific HC genetic program. The first function is suggested by the crucial role of Pou4f3 in ensuring the proper differentiation and survival of all vestibular and auditory HCs (Xiang et al., 1998). The second role of Pou4f3 in contributing to the specificity of Atoh1/Gfi1-driven HC induction is suggested by the cooperation observed between Pou3f2, a related member of the Pou-HD family of TFs, and the bHLH TF Ascl1 in the activation of a neurogenic program in the developing mouse central nervous system (Castro et al., 2006).

We should also note the remarkable similarity between the cocktail of TFs used to convert fibroblasts and hepatocytes into neurons [Ascl1, Brn2 (Pou3f2) and Myt1l] (Vierbuchen et al., 2010; Marro et al., 2011) and the three TFs used in our study, in both cases consisting of a bHLH TF, a Pou-HD TF and a zinc-finger TF. However, whereas the main contribution of Brn2 and Myt1l is to increase the neuronal reprogramming efficiency of Ascl1, our results show that Gfi1 and Pou4f3 are able to radically alter the Atoh1 transcriptional program to promote a distinct HC differentiation program. The work described here thus offers a new model system with which to address the crucial question of how

Development (2015) 142, 1948-1959 doi:10.1242/dev.119149

similar sets of TFs can operate in different modes to implement unique cell fates.

Similarities and differences in the transcriptional profiles of iHCs and native HCs

The ability to obtain purified populations of iHCs using the Myo7a:mVenus reporter line allowed us to generate highly reproducible gene expression profiles for these cells at various phases of their differentiation. Comparison of the iHC transcriptional signature with a core gene expression signature defined for cochlear HCs (500 genes; Cai et al., 2015) reveals that 69% of core HC genes are upregulated by the combined activity of Gfi1, Pou4f3 and Atoh1 in iHCs. When these HC signatures are compared with the set of Atoh1 target genes in cerebellar granule neurons (Klisch et al., 2011), the overlap is much smaller (28% for cochlear HCs and 38% for iHCs), supporting the conclusion that Gfi1, Pou4f3 and Atoh1 activate a HC-specific genetic program. This comparison also highlights the existence of a common set of Atoh1 targets between neurons and HCs, possibly underlying the similar capacity of these cell types to engage in neurotransmission.

The finding that 30% of core HC genes are not activated by the three TFs in iHCs correlates well with the relative immaturity of these cells in culture. In fact, among the ∼30% of HC genes that are not upregulated in iHCs there are several 'deafness' genes encoding late-expressed hair bundle proteins, such as Slc9a9, Fscn2, Gpr98 (Adgrv1), Myo3a and Strc. It is possible that the lack of expression of these genes is due to a developmental delay, as day 12 iHCs (8 days after induction of the three TFs) are likely to be less advanced in development than the neonatal or postnatal day 0 cochlear Atoh1-GFP cells used to define the core HC signature. Another reason might be that the GPA combination can only induce a partial HC phenotype, lacking the activity of additional TFs that are crucial for late HC differentiation. By comparison with the Atonal-driven sensory program in *Drosophila* chordotonal (Ch) neurons (Newton et al., 2012), in which the TF Fd3F acts downstream of Atonal to regulate various genes required for the assembly of mechanosensory cilia, we note that various 'missing' iHC genes are homologs of Fd3F targets in *Drosophila*. These include *Tekt1*, *Wdr63*, *Dnahc6* (*Dnah6*), *Dnahc9* (*Dnah9*) and *Dynlrb2*, which are all involved in axonemal dynein assembly. These genes are also known to be direct or indirect targets of Foxj1, the vertebrate homolog of Fd3F (Stubbs et al., 2008; Jacquet et al., 2009). However, Foxj1 is induced in iHCs by the GPA combination, suggesting that the lack of expression of its targets is due to blockage of its activity in immature iHCs, preventing, for instance, the formation of a proper kinocilium.

We have also scrutinized the list of Atoh1 neuronal targets that are repressed in iHCs, and two genes are worthy of mention – *Gli2* and *Foxm1*, which are known to be crucial for Shh-driven proliferation of CGPs (Flora et al., 2009). Repression of these genes in iHCs illustrates how the combination of Atoh1 with Gfi1 and Pou4f3 leads to key differences in gene expression, with likely functional consequences: whereas Atoh1 induction of Gli2 in CGPs allows these cells to proliferate in response to Shh (Flora et al., 2009), Gli2 repression in iHCs might shield these cells from Shh and contribute to the rapid cell cycle exit that we observed after induction of the three TFs.

Maturation of iHCs *in vitro* requires an adequate cellular environment

Despite their clear progression towards HC differentiation, iHCs failed to develop stereotypical hair bundles *in vitro*. The morphology and length of the espin-rich projections of iHCs were heterogeneous and, although clearly polarized, their position and orientation were variable. This could be due to the inability of iHCs to form a coherent epithelium in culture, preventing the definition of apical-basal polarity required for hair bundle differentiation. By contrast, overexpression of Gfi1, Pou4f3 and Atoh1 in the embryonic chick inner ear induced ectopic but normally polarized HCs, indicating that this TF combination does not interfere with the normal progression of HC differentiation. These findings suggest that environmental factors and/or a proper cellular context are essential to achieve complete HC differentiation *in vitro*.

With regard to environmental factors, our data show that inhibition of Notch signaling or addition of RA can improve iHC differentiation. Notch activity is known to prevent HC specification in the inner ear (Kiernan, 2013), and our microarray data reveal that Notch signaling is active during iHC formation (supplementary material Fig. S8). The addition of a Notch inhibitor is therefore expected to facilitate iHC formation, and our results confirm this. The activity of RA was also expected to increase iHC differentiation, following previous findings that the addition of RA to chick otic vesicles or mouse organ of Corti explants results in early onset of HC differentiation and supernumerary HCs (Represa et al., 1990; Kelley et al., 1993). Little is known about how RA signaling leads to this effect, but our work might offer some cues as to the underlying molecular mechanisms. For instance, the finding that RA addition represses Hes1 expression raises the hypothesis that this could relieve Atoh1 from its antagonizing activity (Zheng et al., 2000a) and lead to an increased efficiency of iHC generation.

Concerning the requirement for an adequate multicellular organization for iHC differentiation, we have used several strategies to address this issue, either by co-culturing iHCs with otic-derived mesenchymal cells or by using various synthetic scaffolds to grow dissociated EB cells, but never observed a proper epithelial organization of iHC aggregates *in vitro*. A possible explanation is the absence of supporting cells (SCs) in iHC cultures, which are necessary *in vivo* to establish specific cell-cell adhesion with HCs. In fact, our data suggest that GPA induction of iHCs does not lead to the concomitant induction of SCs. Although iHCs expressed Sox2, typical supporting cell markers such as Prox1 and E-cadherin (cadherin 1) were absent in Dox-treated EBs (data not shown), and analysis of iHC transcriptomes confirms the lack of expression of SC genes [*Gfap*, neurotrophin receptor P75 (*Ngfr*), *GLAST* (*Slc1a3*) and *Jag1*]. This suggests that the combined activation of Gfi1, Pou4f3 and Atoh1 promotes direct conversion to an HC fate, bypassing the bipotent progenitor cell state that normally precedes SC and HC formation *in vivo*.

In summary, we report the first successful and efficient method for direct conversion of mESC-derived progenitors into iHCs, providing a proof-of-concept for HC programming. This simple and rapid method offers an alternative approach to produce large numbers of HC-like cells *in vitro*. Further work will aim to investigate whether the forced expression of Gfi1-Pou4f3-Atoh1 could also direct other somatic cell types towards HC differentiation, and how these three TFs regulate HC commitment and differentiation.

MATERIALS AND METHODS

mESC maintenance and differentiation

Ainv15, iAtoh1, iGPA and iGPA-Myo7a:mVenus mESC lines were maintained on gelatin-coated dishes in DMEM (Invitrogen) supplemented with 10% ES-qualified FBS (Invitrogen), 1 mM 2-mercaptoethanol and 2 ng/ml LIF. For EB differentiation, mESCs were trypsinized using 0.25%

Development (2015) 142, 1948-1959 doi:10.1242/dev.119149

trypsin-EDTA (Invitrogen) and resuspended on bacterial-grade Petri dishes in the same medium without LIF. Medium supplementation with 2 µg/ml Dox, 1 µM RA and 10 nM LY411575 was performed as described in the figures. For further details, see the supplementary Materials and Methods.

Generation of iAtoh1 and iGPA lines

Ainv15 mESC cells (4×10^6) were electroporated (Gene Pulser II, Bio-Rad; 250 V,500 µF) with 20 µg pTurbo-Cre and 20 µg Atoh1Plox or GPAPlox vectors (see supplementary Materials and Methods). Cells were subsequently plated on neomycin-resistant and mitotically inactivated MEF feeder cells in DMEM medium supplemented with 350 µg/ml G418. Individual colonies were picked 10-14 days after electroporation.

RNA extraction, microarray analysis and quantitative PCR

Total RNA was extracted from 10^6 EB-derived cells subjected to different culture conditions using the High Pure RNA Isolation kit (Roche Diagnostics) for hybridization on Mouse Genome 2.1 ST Arrays Strip (Affymetrix). Log_2 expression values of transcripts were imported to Chipster 2.4 (Kallio et al., 2011) for data analysis. The GEO accession number for the mRNA microarray data is GSE60352. For further details of microarray sample preparation and data analysis see the supplementary Materials and Methods.

To perform quantitative real-time PCR, first-strand cDNA was synthesized from 1 µg total RNA using Superscript II reverse transcriptase (Invitrogen) and random hexamers. Real-time PCR was performed with SYBR Green and exon-spanning primers in 7500 and ViiA 7 real-time PCR systems (Applied Biosystems). Further details, including primer sequences, are provided in the supplementary Materials and Methods.

Immunocytochemistry, imaging and cell counts

EBs and electroporated embryos were processed for immunocytochemistry as described in the supplementary Materials and Methods using the primary antibodies listed in supplementary material Table S2 and Alexa Fluor-conjugated secondary antibodies (Molecular Probes) and 0.15% DAPI (Sigma-Aldrich). EdU incorporation employed the Click-iT EdU Alexa Fluor 488 Flow Cytometry Assay Kit (Molecular Probes).

Fluorescent and bright-field images of fixed sections and cells were captured and processed as described in the supplementary Materials and Methods. The number of cells expressing Myo7a, espin, Pou4f3 or Venus was quantified among total induced cells or among the total number of cells in EBs in four to five randomly selected fields using Photoshop CS Cell Counter software (Adobe) as described in the supplementary Materials and Methods.

Flow cytometry

Live cell analysis and intracellular staining of fixed cells were performed as described in the supplementary Materials and Methods using Myo7a and GFP primary antibodies (supplementary material Table S2) and Alexa Fluor-conjugated secondary antibodies (Molecular Probes). Data were analyzed with FlowJo software (Tree Star).

FM1-43 uptake assay

iHC fast permeation to FM1-43 dye [*N*-(3-triethylammoniumpropyl)-4-(4-(dibutylamino)styryl)pyridinium dibromide] (Molecular Probes) was assessed as described in the supplementary Materials and Methods.

Scanning electron microscopy

Co-cultures of EB-derived progenitors and mitotically inactivated chicken utricle mesenchyme treated with Dox and RA were processed for SEM using a JEOL 6700F microscope as described in the supplementary Materials and Methods.

Chicken otic cup electroporation

Electroporations of the inner ear were performed at E2 using Electro Square Porator TM ECM830 (BTX) as described (Freeman et al., 2012). The Tol2 transposon vectors were electroporated at a final concentration of 1 µg/µl. For details, see the supplementary Materials and Methods.

Statistics

All data are expressed as mean±s.e.m. and statistical significance was assessed using an unpaired Student's *t*-test. For all statistics, data from at least three biologically independent experiments were used. Data and graphs were tabulated and prepared using Microsoft Excel and GraphPad Prism software. $P<0.05$ was considered statistically significant.

Acknowledgements

We thank Tiantian Cai and Andrew Groves for sharing unpublished RNA-seq data from Atoh1-GFP HCs; Jörg Becker/IGC Gene Expression Unit for technical support with microarray analysis; Andrew Forge and Telmo Nunes for SEM support; Sara Ferreira, IMM bioimaging and flow cytometry facilities for technical help; Fernando Giraldez for critical reading of the manuscript; and Filipe Vilas-Boas for helpful discussions.

Competing interests

The authors declare no competing or financial interests.

Author contributions

A.C. conceived, performed and analyzed the experiments and wrote the paper. L.S.-G. performed the chick electroporations. S.J. prepared the inactivated utricle periodic mesenchyme cells. J.E.G. and N.D. provided scientific and technical advice for some experiments. D.H. conceived and supervised the study and wrote the paper.

Funding

This work was supported by Fundação para a Ciência e Tecnologia, Portugal [PTDC/SAU-NEU/71310/2006, SFRH/BD/38461/2007 to A.C.]. A.C. was also a recipient of an EMBO Short-Term Fellowship during her stay at the UCL Ear Institute. S.J. is funded by a UCL Impact Studentship to J.E.G. Work in N.D.'s lab is supported by the BBSRC [BB/L003163/1].

Supplementary material

Supplementary material available online at
http://dev.biologists.org/lookup/suppl/doi:10.1242/dev.119149/-/DC1

References

Ben-Arie, N., Bellen, H. J., Armstrong, D. L., McCall, A. E., Gordadze, P. R., Guo, Q., Matzuk, M. M. and Zoghbi, H. Y. (1997). Math1 is essential for genesis of cerebellar granule neurons. *Nature* **390**, 169-172.

Ben-Arie, N., Hassan, B. A., Bermingham, N. A., Malicki, D. M., Armstrong, D., Matzuk, M., Bellen, H. J. and Zoghbi, H. Y. (2000). Functional conservation of atonal and Math1 in the CNS and PNS. *Development* **127**, 1039-1048.

Bermingham, N. A., Hassan, B. A., Price, S. D., Vollrath, M. A., Ben-Arie, N., Eatock, R. A., Bellen, H. J., Lysakowski, A. and Zoghbi, H. Y. (1999). Math1: an essential gene for the generation of inner ear hair cells. *Science* **284**, 1837-1841.

Bermingham, N. A., Hassan, B. A., Wang, V. Y., Fernandez, M., Banfi, S., Bellen, H. J., Fritzsch, B. and Zoghbi, H. Y. (2001). Proprioceptor pathway development is dependent on MATH1. *Neuron* **30**, 411-422.

Bjerknes, M. and Cheng, H. (2010). Cell Lineage metastability in Gfi1-deficient mouse intestinal epithelium. *Dev. Biol.* **345**, 49-63.

Boeda, B., Weil, D. and Petit, C. (2001). A specific promoter of the sensory cells of the inner ear defined by transgenesis. *Hum. Mol. Genet.* **10**, 1581-1589.

Cai, T., Seymour, M. L., Zhang, H., Pereira, F. A. and Groves, A. K. (2013). Conditional deletion of Atoh1 reveals distinct critical periods for survival and function of hair cells in the organ of Corti. *J. Neurosci.* **33**, 10110-10122.

Cai, T., Jen, H. I., Kang, H., Klisch, T. J., Zoghbi, H. Y. and Groves, A. K. (2015). Characterization of the transcriptome of nascent hair cells and identification of direct targets of the atoh1 transcription factor. *J. Neurosci.* **35**, 5870-5883.

Castro, D. S., Skowronska-Krawczyk, D., Armant, O., Donaldson, I. J., Parras, C., Hunt, C., Critchley, J. A., Nguyen, L., Gossler, A., Göttgens, B. et al. (2006). Proneural bHLH and Brn proteins coregulate a neurogenic program through cooperative binding to a conserved DNA motif. *Dev. Cell* **11**, 831-844.

Chen, P., Johnson, J. E., Zoghbi, H. Y. and Segil, N. (2002). The role of Math1 in inner ear development: uncoupling the establishment of the sensory primordium from hair cell fate determination. *Development* **129**, 2495-2505.

Davies, S. and Forge, A. (1987). Preparation of the mammalian organ of Corti for scanning electron microscopy. *J. Microsc.* **147**, 89-101.

El-Amraoui, A., Sahly, I., Picaud, S., Sahel, J., Abitbol, M. and Petit, C. (1996). Human Usher 1B/mouse shaker-1: the retinal phenotype discrepancy explained by the presence/absence of myosin VIIA in the photoreceptor cells. *Hum. Mol. Genet.* **5**, 1171-1178.

Flora, A., Klisch, T. J., Schuster, G. and Zoghbi, H. Y. (2009). Deletion of Atoh1 disrupts Sonic Hedgehog signaling in the developing cerebellum and prevents medulloblastoma. *Science* **326**, 1424-1427.

Freeman, S., Chrysostomou, E., Kawakami, K., Takahashi, Y. and Daudet, N. (2012). Tol2-mediated gene transfer and in ovo electroporation of the otic placode:

a powerful and versatile approach for investigating embryonic development and regeneration of the chicken inner ear. *Methods Mol. Biol.* **916**, 127-139.
Fritzsch, B., Jahan, I., Pan, N. and Elliott, K. L. (2015). Evolving gene regulatory networks into cellular networks guiding adaptive behavior: an outline how single cells could have evolved into a centralized neurosensory system. *Cell Tissue Res.* **359**, 295-313.
Gale, J. E., Marcotti, W., Kennedy, H. J., Kros, C. J. and Richardson, G. P. (2001). FM1-43 dye behaves as a permeant blocker of the hair-cell mechanotransducer channel. *J. Neurosci.* **21**, 7013-7025.
Hume, C. R., Bratt, D. L. and Oesterle, E. C. (2007). Expression of LHX3 and SOX2 during mouse inner ear development. *Gene Expr. Patterns* **7**, 798-807.
Jacquet, B. V., Salinas-Mondragon, R., Liang, H., Therit, B., Buie, J. D., Dykstra, M., Campbell, K., Ostrowski, L. E., Brody, S. L. and Ghashghaei, H. T. (2009). FoxJ1-dependent gene expression is required for differentiation of radial glia into ependymal cells and a subset of astrocytes in the postnatal brain. *Development* **136**, 4021-4031.
Jarman, A. P. and Groves, A. K. (2013). The role of Atonal transcription factors in the development of mechanosensitive cells. *Semin. Cell Dev. Biol.* **24**, 438-447.
Kallio, M. A., Tuimala, J. T., Hupponen, T., Klemelä, P., Gentile, M., Scheinin, I., Koski, M., Käki, J. and Korpelainen, E. I. (2011). Chipster: user-friendly analysis software for microarray and other high-throughput data. *BMC Genomics* **12**, 507.
Kelley, M. W., Xu, X. M., Wagner, M. A., Warchol, M. E. and Corwin, J. T. (1993). The developing organ of Corti contains retinoic acid and forms supernumerary hair cells in response to exogenous retinoic acid in culture. *Development* **119**, 1041-1053.
Kelly, M. C., Chang, Q., Pan, A., Lin, X. and Chen, P. (2012). Atoh1 directs the formation of sensory mosaics and induces cell proliferation in the postnatal mammalian cochlea in vivo. *J. Neurosci.* **32**, 6699-6710.
Kiernan, A. E. (2013). Notch signaling during cell fate determination in the inner ear. *Semin. Cell Dev. Biol.* **24**, 470-479.
Kim, P., Helms, A. W., Johnson, J. E. and Zimmerman, K. (1997). XATH-1, a vertebrate homolog of Drosophila atonal, induces a neuronal differentiation within ectodermal progenitors. *Dev. Biol.* **187**, 1-12.
Klisch, T. J., Xi, Y., Flora, A., Wang, L. G., Li, W. and Zoghbi, H. Y. (2011). In vivo Atoh1 targetome reveals how a proneural transcription factor regulates cerebellar development. *Proc. Natl. Acad. Sci. USA* **108**, 3288-3293.
Koehler, K. R., Mikosz, A. M., Molosh, A. I., Patel, D. and Hashino, E. (2013). Generation of inner ear sensory epithelia from pluripotent stem cells in 3D culture. *Nature* **500**, 217-221.
Kyba, M., Perlingeiro, R. C. R. and Daley, G. Q. (2002). HoxB4 confers definitive lymphoid-myeloid engraftment potential on embryonic stem cell and yolk sac hematopoietic progenitors. *Cell* **109**, 29-37.
Lanz, T. A., Hosley, J. D., Adams, W. J. and Merchant, K. M. (2004). Studies of Aβ pharmacodynamics in the brain, cerebrospinal fluid, and plasma in young (plaque-free) Tg2576 mice using the γ-secretase inhibitor N2-[(2S)-2-(3,5-difluorophenyl)-2-hydroxyethanoyl]-N1-[(7S)-5-methyl-6-oxo-6,7-dihydro-5H-dibenzo[b,d]azepin-7-yl]-L-alaninamide (LY-411575). *J. Pharmacol. Exp. Ther.* **309**, 49-55.
Li, M., Pevny, L., Lovell-Badge, R. and Smith, A. (1998). Generation of purified neural precursors from embryonic stem cells by lineage selection. *Curr. Biol.* **8**, 971-974.
Liu, Z., Dearman, J. A., Cox, B. C., Walters, B. J., Zhang, L., Ayrault, O., Zindy, F., Gan, L., Roussel, M. F. and Zuo, J. (2012). Age-dependent in vivo conversion of mouse cochlear pillar and Deiters' cells to immature hair cells by Atoh1 ectopic expression. *J. Neurosci.* **32**, 6600-6610.
Malgrange, B., Belachew, S., Thiry, M., Nguyen, L., Rogister, B., Alvarez, M.-L., Rigo, J.-M., Van De Water, T. R., Moonen, G. and Lefebvre, P. P. (2002). Proliferative generation of mammalian auditory hair cells in culture. *Mech. Dev.* **112**, 79-88.
Maricich, S. M., Wellnitz, S. A., Nelson, A. M., Lesniak, D. R., Gerling, G. J., Lumpkin, E. A. and Zoghbi, H. Y. (2009). Merkel cells are essential for light-touch responses. *Science* **324**, 1580-1582.
Marro, S., Pang, Z. P., Yang, N., Tsai, M.-C., Qu, K., Chang, H. Y., Südhof, T. C. and Wernig, M. (2011). Direct lineage conversion of terminally differentiated hepatocytes to functional neurons. *Cell Stem Cell* **9**, 374-382.
Matei, V., Pauley, S., Kaing, S., Rowitch, D., Beisel, K. W., Morris, K., Feng, F., Jones, K., Lee, J. and Fritzsch, B. (2005). Smaller inner ear sensory epithelia in Neurog1 null mice are related to earlier hair cell cycle exit. *Dev. Dyn.* **234**, 633-650.
Mulvaney, J. and Dabdoub, A. (2012). Atoh1, an essential transcription factor in neurogenesis and intestinal and inner ear development: function, regulation, and context dependency. *J. Assoc. Res. Otolaryngol.* **13**, 281-293.
Newton, F. G., zur Lage, P. I., Karak, S., Moore, D. J., Göpfert, M. C. and Jarman, A. P. (2012). Forkhead transcription factor Fd3F cooperates with Rfx to regulate a gene expression program for mechanosensory cilia specialization. *Dev. Cell* **22**, 1221-1233.
Ninkina, N. N., Stevens, G. E. M., Wood, J. N. and Richardson, W. D. (1993). A novel Brn3-like POU transcription factor expressed in subsets of rat sensory and spinal cord neurons. *Nucleic Acids Res.* **21**, 3175-3182.
Oshima, K., Shin, K., Diensthuber, M., Peng, A. W., Ricci, A. J. and Heller, S. (2010). Mechanosensitive hair cell-like cells from embryonic and induced pluripotent stem cells. *Cell* **141**, 704-716.
Pan, N., Jahan, I., Kersigo, J., Duncan, J. S., Kopecky, B. and Fritzsch, B. (2012). A novel Atoh1 "self-terminating" mouse model reveals the necessity of proper Atoh1 level and duration for hair cell differentiation and viability. *PLoS ONE* **7**, e30358.
Represa, J., Sanchez, A., Miner, C., Lewis, J. and Giraldez, F. (1990). Retinoic acid modulation of the early development of the inner-ear is associated with the control of C-Fos expression. *Development* **110**, 1081-1090.
Rose, M. F., Ren, J., Ahmad, K. A., Chao, H.-T., Klisch, T. J., Flora, A., Greer, J. J. and Zoghbi, H. Y. (2009). Math1 is essential for the development of hindbrain neurons critical for perinatal breathing. *Neuron* **64**, 341-354.
Ruben, R. J. (1967). Development of the inner ear of the mouse: a radioautographic study of terminal mitoses. *Acta Otolaryngol.* **220**, 1-44.
Sage, C., Huang, M., Vollrath, M. A., Brown, M. C., Hinds, P. W., Corey, D. P., Vetter, D. E. and Chen, Z.-Y. (2006). Essential role of retinoblastoma protein in mammalian hair cell development and hearing. *Proc. Natl. Acad. Sci. USA* **103**, 7345-7350.
Sekerkova, G., Zheng, L., Loomis, P. A., Mugnaini, E. and Bartles, J. R. (2006). Espins and the actin cytoskeleton of hair cell stereocilia and sensory cell microvilli. *Cell. Mol. Life Sci.* **63**, 2329-2341.
Shroyer, N. F., Wallis, D., Venken, K. J. T., Bellen, H. J. and Zoghbi, H. Y. (2005). Gfi1 functions downstream of Math1 to control intestinal secretory cell subtype allocation and differentiation. *Genes Dev.* **19**, 2412-2417.
Siemens, J., Lillo, C., Dumont, R. A., Reynolds, A., Williams, D. S., Gillespie, P. G. and Müller, U. (2004). Cadherin 23 is a component of the tip link in hair-cell stereocilia. *Nature* **428**, 950-955.
Smyth, G. K. (2004). Linear models and empirical bayes methods for assessing differential expression in microarray experiments. *Stat. Appl. Genet. Mol. Biol.* **3**, 1-25.
Stubbs, J. L., Oishi, I., Izpisúa Belmonte, J. C. and Kintner, C. (2008). The forkhead protein Foxj1 specifies node-like cilia in Xenopus and zebrafish embryos. *Nat. Genet.* **40**, 1454-1460.
Szymczak, A. L., Workman, C. J., Wang, Y., Vignali, K. M., Dilioglou, S., Vanin, E. F. and Vignali, D. A. A. (2004). Correction of multi-gene deficiency in vivo using a single 'self-cleaving' 2A peptide–based retroviral vector. *Nat. Biotechnol.* **22**, 589-594.
Takahashi, Y., Watanabe, T., Nakagawa, S., Kawakami, K. and Sato, Y. (2008). Transposon-mediated stable integration and tetracycline-inducible expression of electroporated transgenes in chicken embryos. *Methods Cell Biol.* **87**, 271-280.
Ting, D. T., Kyba, M. and Daley, G. Q. (2005). Inducible transgene expression in mouse stem cells. *Methods Mol. Med.* **105**, 23-46.
Tsuda, H., Jafar-Nejad, H., Patel, A. J., Sun, Y., Chen, H.-K., Rose, M. F., Venken, K. J. T., Botas, J., Orr, H. T., Bellen, H. J. et al. (2005). The AXH domain of Ataxin-1 mediates neurodegeneration through its interaction with Gfi-1/senseless proteins. *Cell* **122**, 633-644.
Vierbuchen, T., Ostermeier, A., Pang, Z. P., Kokubu, Y., Südhof, T. C. and Wernig, M. (2010). Direct conversion of fibroblasts to functional neurons by defined factors. *Nature* **463**, 1035-1041.
Wallis, D., Hamblen, M., Zhou, Y., Venken, K. J. T., Schumacher, A., Grimes, H. L., Zoghbi, H. Y., Orkin, S. H. and Bellen, H. J. (2003). The zinc finger transcription factor Gfi1, implicated in lymphomagenesis, is required for inner ear hair cell differentiation and survival. *Development* **130**, 221-232.
Wang, S. W., Mu, X., Bowers, W. J., Kim, D. S., Plas, D. J., Crair, M. C., Federoff, H. J., Gan, L. and Klein, W. H. (2002). Brn3b/Brn3c double knockout mice reveal an unsuspected role for Brn3c in retinal ganglion cell axon outgrowth. *Development* **129**, 467-477.
Warchol, M. E. (2011). Sensory regeneration in the vertebrate inner ear: differences at the levels of cells and species. *Hear. Res.* **273**, 72-79.
Woods, C., Montcouquiol, M. and Kelley, M. W. (2004). Math1 regulates development of the sensory epithelium in the mammalian cochlea. *Nat. Neurosci.* **7**, 1310-1318.
Xiang, M., Zhou, L., Macke, J. P., Yoshioka, T., Hendry, S. H., Eddy, R. L., Shows, T. B. and Nathans, J. (1995). The Brn-3 family of POU-domain factors: primary structure, binding specificity, and expression in subsets of retinal ganglion cells and somatosensory neurons. *J. Neurosci.* **15**, 4762-4785.
Xiang, M., Gan, L., Li, D., Chen, Z.-Y., Zhou, L., O'Malley, B. W., Jr, Klein, W. and Nathans, J. (1997). Essential role of POU-domain factor Brn-3c in auditory and vestibular hair cell development. *Proc. Natl. Acad. Sci. USA* **94**, 9445-9450.
Xiang, M., Gao, W.-Q., Hasson, T. and Shin, J. J. (1998). Requirement for Brn-3c in maturation and survival, but not in fate determination of inner ear hair cells. *Development* **125**, 3935-3946.
Yang, Q., Bermingham, N. A., Finegold, M. J. and Zoghbi, H. Y. (2001). Requirement of Math1 for secretory cell lineage commitment in the mouse intestine. *Science* **294**, 2155-2158.
Zheng, J. L. and Gao, W.-Q. (2000). Overexpression of Math1 induces robust production of extra hair cells in postnatal rat inner ears. *Nat. Neurosci.* **3**, 580-586.
Zheng, J. L., Shou, J. Y., Guillemot, F., Kageyama, R. and Gao, W. Q. (2000a). Hes1 is a negative regulator of inner ear hair cell differentiation. *Development* **127**, 4551-4560.
Zheng, L., Sekerková, G., Vranich, K., Tilney, L. G., Mugnaini, E. and Bartles, J. R. (2000b). The deaf jerker mouse has a mutation in the gene encoding the espin actin-bundling proteins of hair cell stereocilia and lacks espins. *Cell* **102**, 377-385.

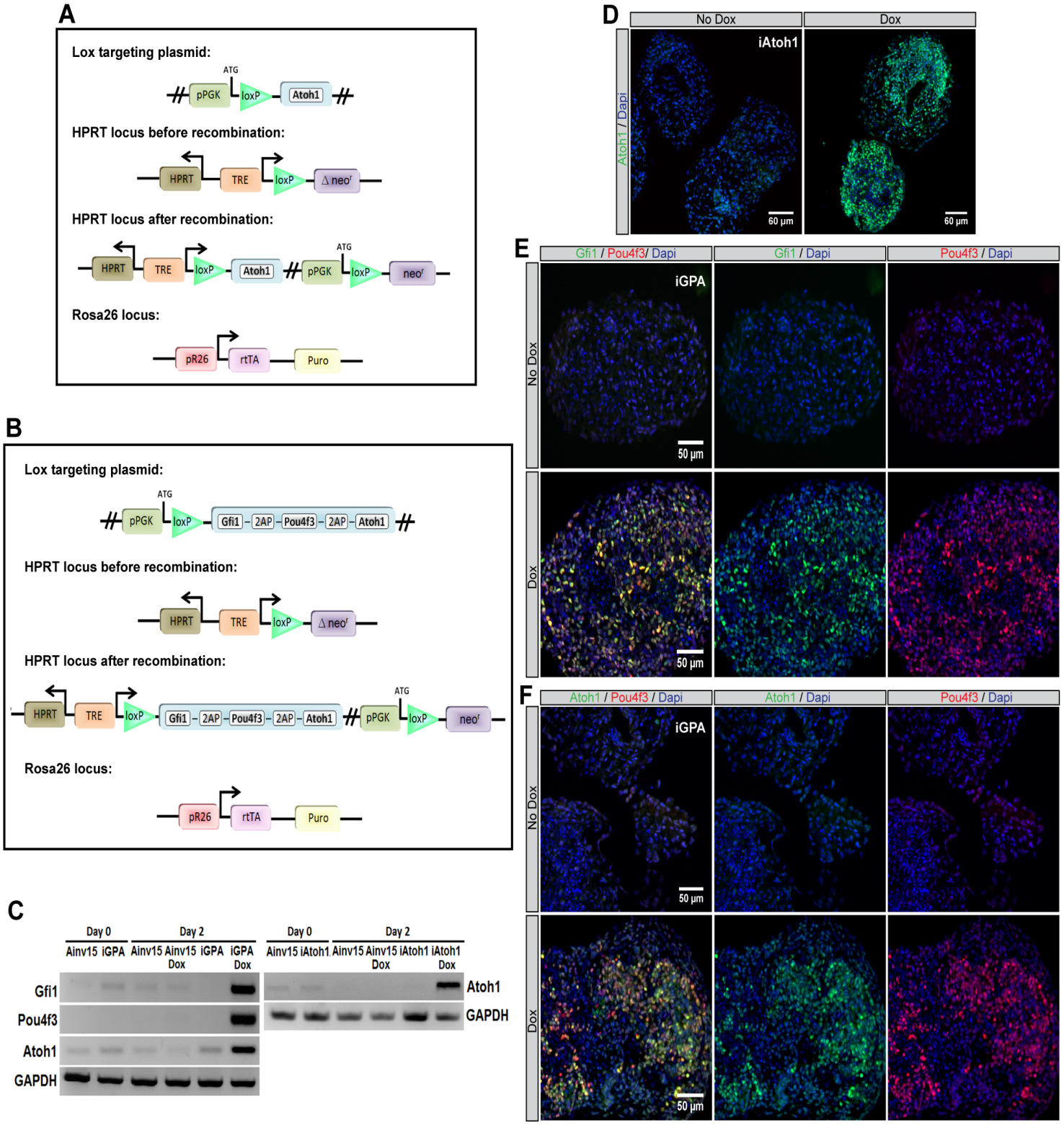

Fig. S1. Generation and characterization of iAtoh1 and iGPA ES lines.

(A and B) Schematic representation of experimental procedures used for the generation of mESC lines in which Doxycycline-induced expression of Atoh1 (A) and co-expression of Gfi1, Pou4f3 and Atoh1 (B) can be achieved.

(C) RT-PCR analysis reveals strong expression of *Gfi1*, *Pou4f3* and *Atoh1* mRNAs after 48h of 2µg/ml Dox treatment in the iGPA line, but not in the parental Ainv15 line. Similarly, the iAtoh1 line also shows increased *Atoh1* expression upon Dox treatment.
(D) Immunostaining for Atoh1 expression in day 6 EBs generated from iAtoh1 mESCs, cultured with or without Dox for 24h.
(E and F) Immunostaining analysis of Pou4f3/Gfi1 (E) and Pou4f3/Atoh1 (F) in EBs derived from iGPA mESCs in the presence or absence of Dox for 24h.
Abbrevaitions: pPGK, phospho-glycero-kinase promoter; HPRT, hypoxanthine phosphoribosyltransferase 1 gene; TRE, tetracycline responsive element; rtTA, reverse tetracycline transactivator; Puro, puromycin resistance gene; pR26, promoter of the ROSA26 locus; 2AP, 2A peptide sequence; ATG, start codon for the neo gene; loxP, Cre-recombinase recognition sequence; Δ neo^r, deletion mutant of the neomycin (G418) resistance gene; //, plasmid sequence.

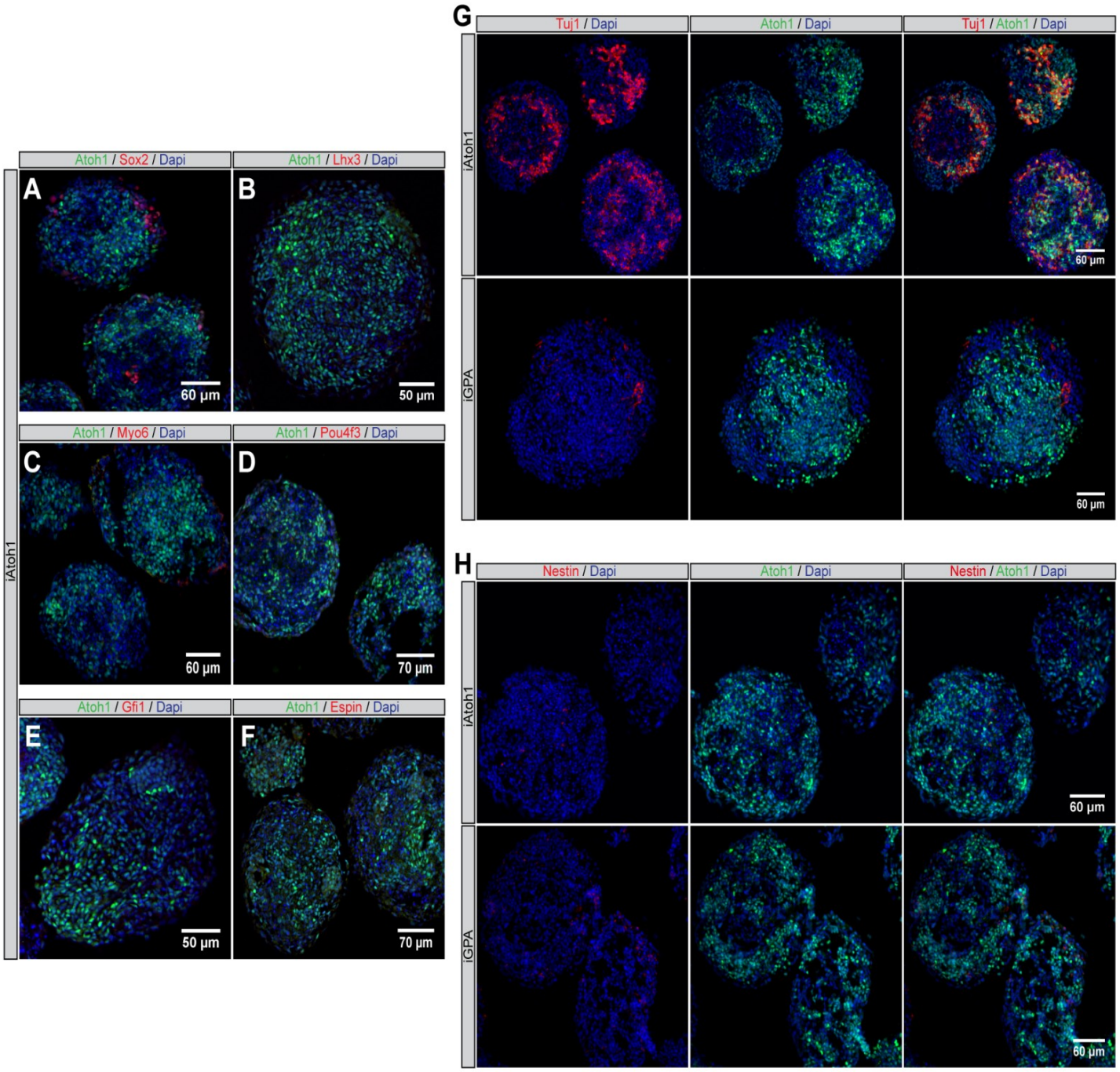

Fig. S2. Forced expression of Atoh1 promotes neuronal differentiation but not hair cell fate.

(A-F) Immunostaining for several HC specific markers performed in day 8 iAtoh1-derived EBs previously exposed to Dox for 4 days. Among induced Atoh1^{+} cells, no significant up-regulation was observed for Sox2 (A), Lhx3 (B), Myo6 (C), Pou4f3 (D), Gfi1 (E) and Espin (F).

(G, H) Immunostaining for Tuj1 and Nestin in Day 8 EBs derived from iAtoh1 and iGPA mESCs, after 4 days of Dox induction. Tuj1+ neurons can only be detected in iAtoh1 EBs, not in iGPA EBs. Nestin is not induced in any of the cases.

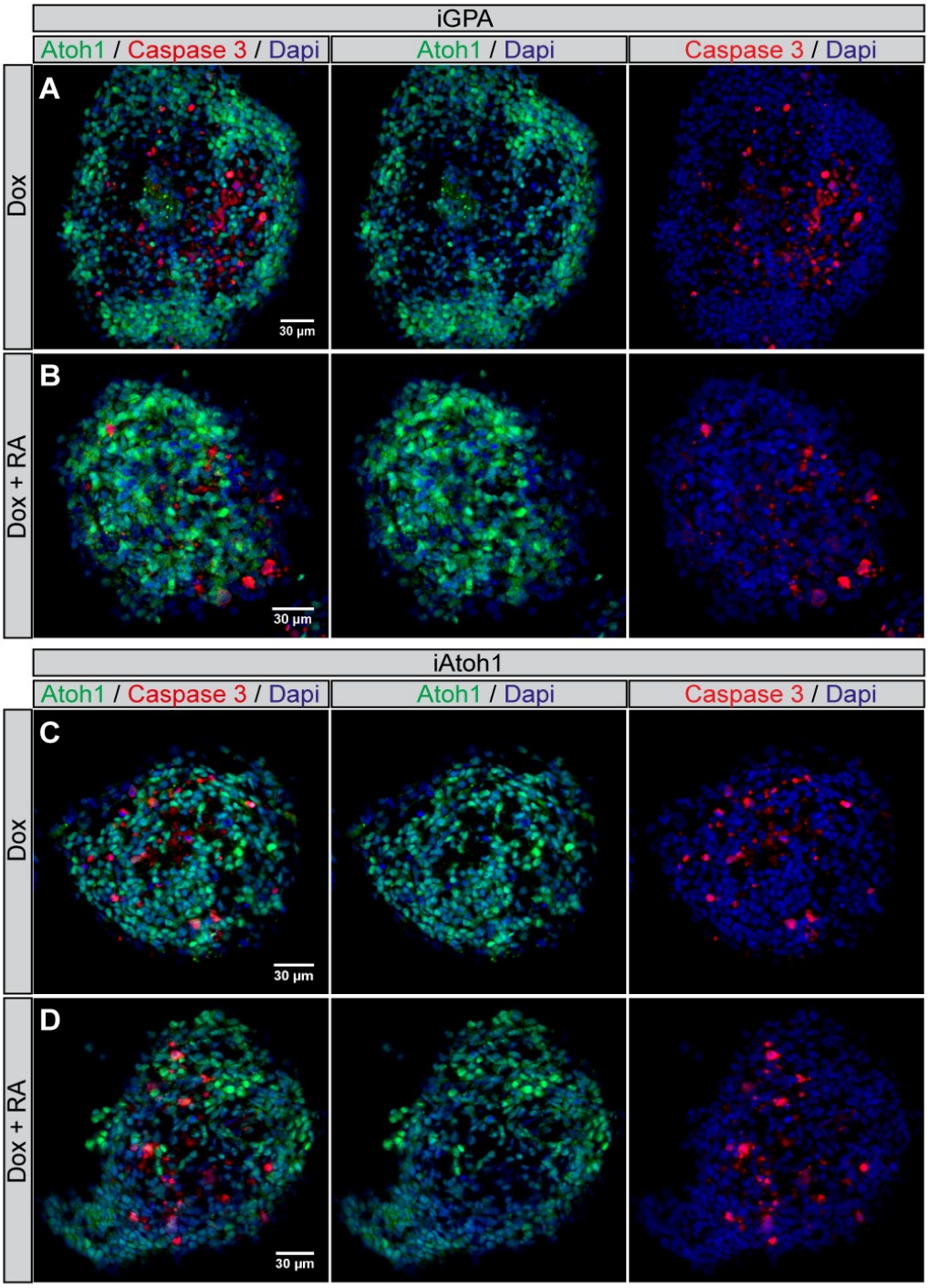

Fig. S3. Cells overexpressing Atoh1 and GPA in Dox-induced EBs do not show differences in cell survival.

Immunostaining analysis for activated Caspase 3 and Atoh1 performed in iGPA-derived EBs (A and B) and in iAtoh1-derived EBs (C and D) at day 8. Quantification of Atoh1+/aCas3+ cells in iAtoh1 (2,64 ± 1,4%) and iGPA (2,59 ± 1,2%) EBs revealed no significant difference between the two conditions.

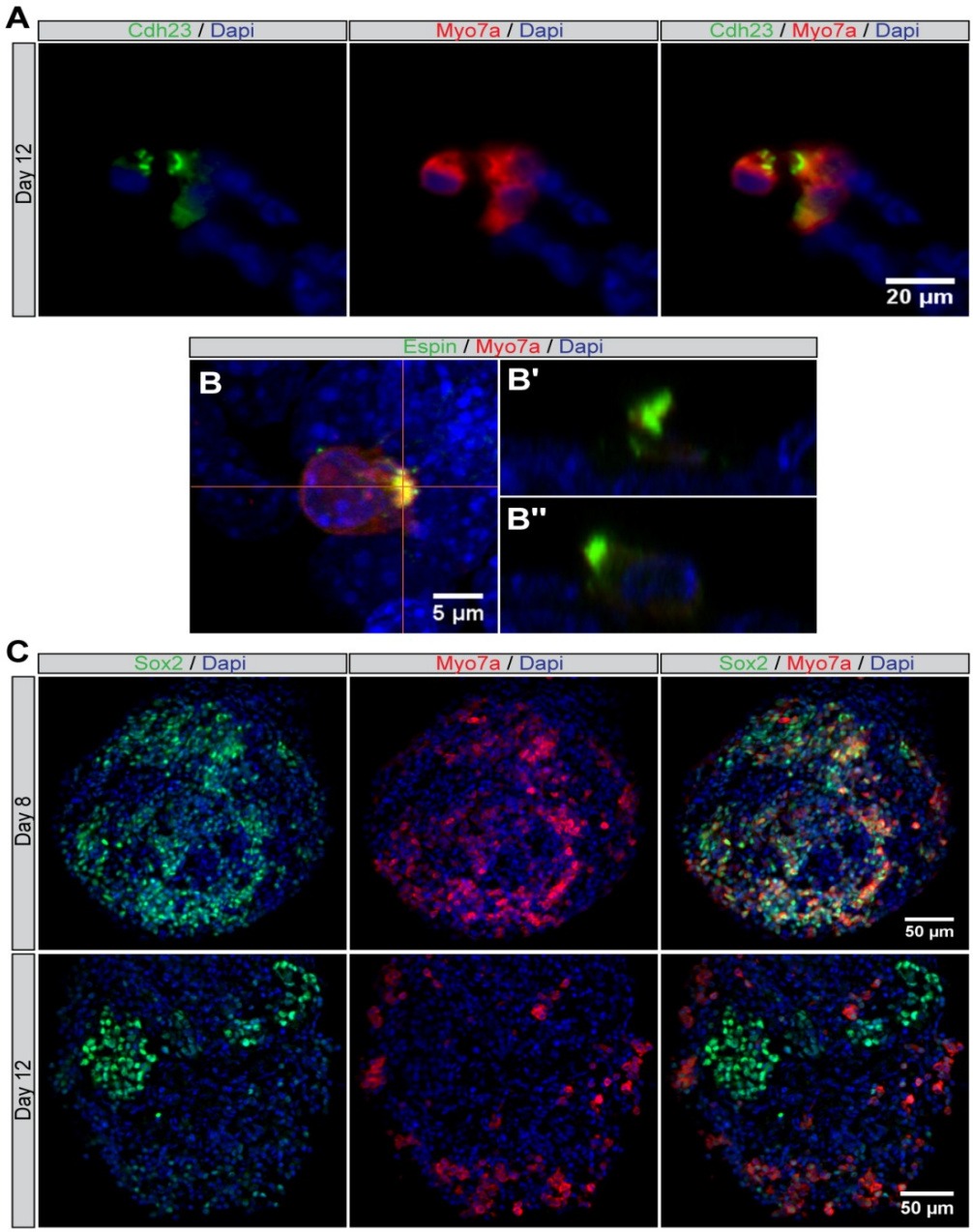

Fig. S4. iHC progenitors can differentiate and develop hair bundle-like structures.
(A) Immunostaining for Cdh23 and Myo7a in day 12 iGPA EBs exposed to Dox during 8 days.
(B) High magnification views of the hair bundle-like protrusions labelled with Myo7a and Espin in iHCs co-cultured with embryonic chicken utricle mesenchymal cells (protocol described in Figure 3E). Note that B' and B'' are orthogonal views showing Espin^{+} structures oriented to the top of the culture dish.
(C) Immunostaining for Sox2 in iGPA-derived EBs reveals a decrease in its expression in Myo7a^{+} cells from day 8 to day 12.

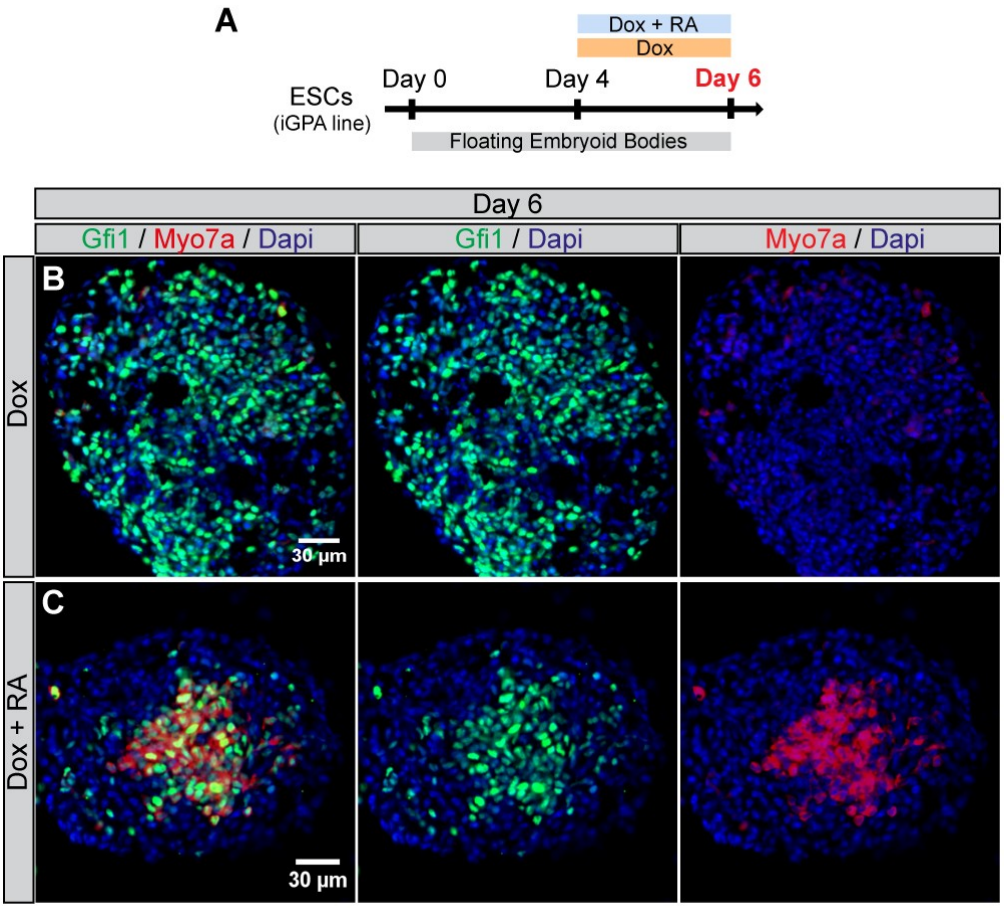

Fig. S5. RA promotes early onset of HC differentiation.

(A) Schematic diagram of the ES cell differentiation protocol through EB formation, including a 2 day period of Dox induction.

(B and C) Immunostaining analysis of Myo7a and Gfi1 expression performed in EBs harvested at day 6, showing strong up-regulation of Myo7a only in the Dox + RA condition (B) and not with Dox stimulation alone (C).

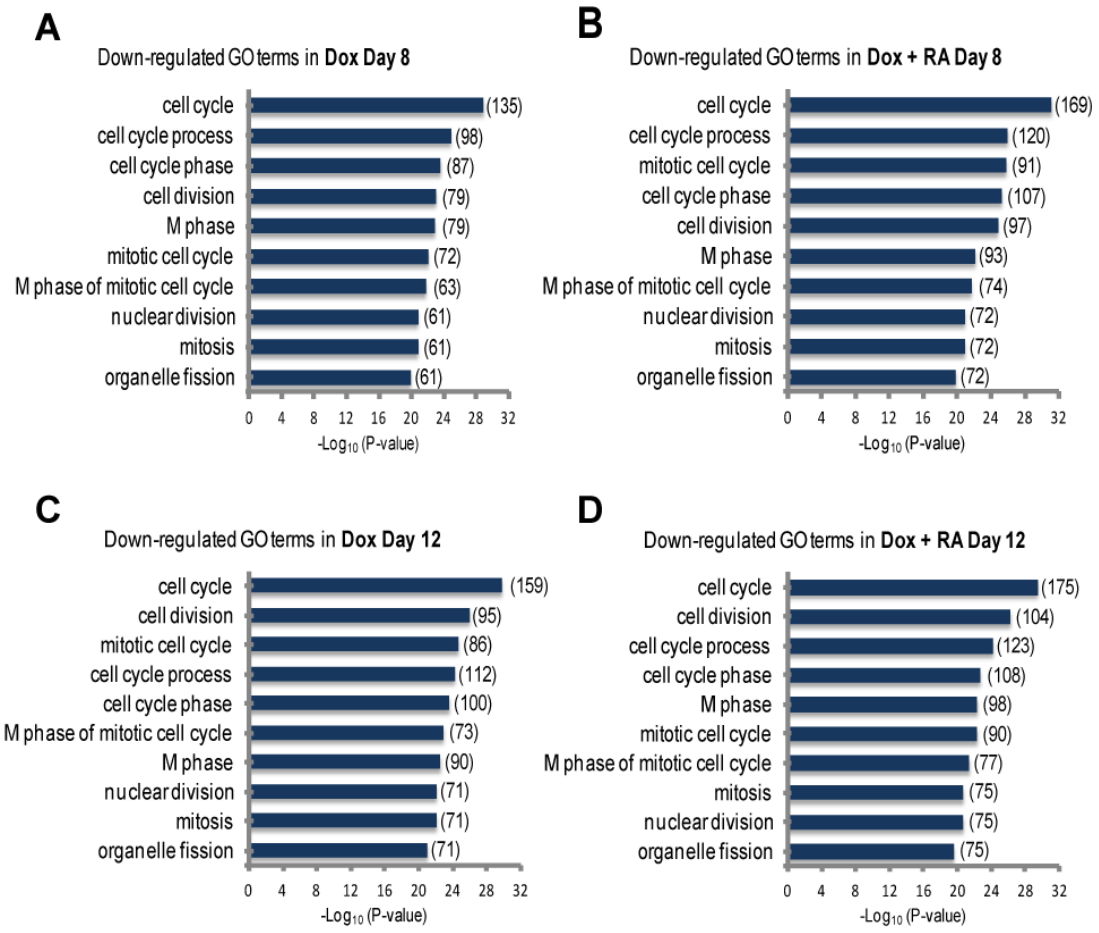

Fig. S6. Analyses of significant down-regulated genes in iHC transcriptomes.
(A-D) Gene ontology (GO) analysis using DAVID functional annotation tool for the significant down-regulated genes detected in the four different iHC groups (expression fold changes > 2, *P*-value < 0,01), when compared to untreated cells at day 8 (A and B) and at day 12 (C and D). The number of up-regulated genes included in each GO functional term is shown.

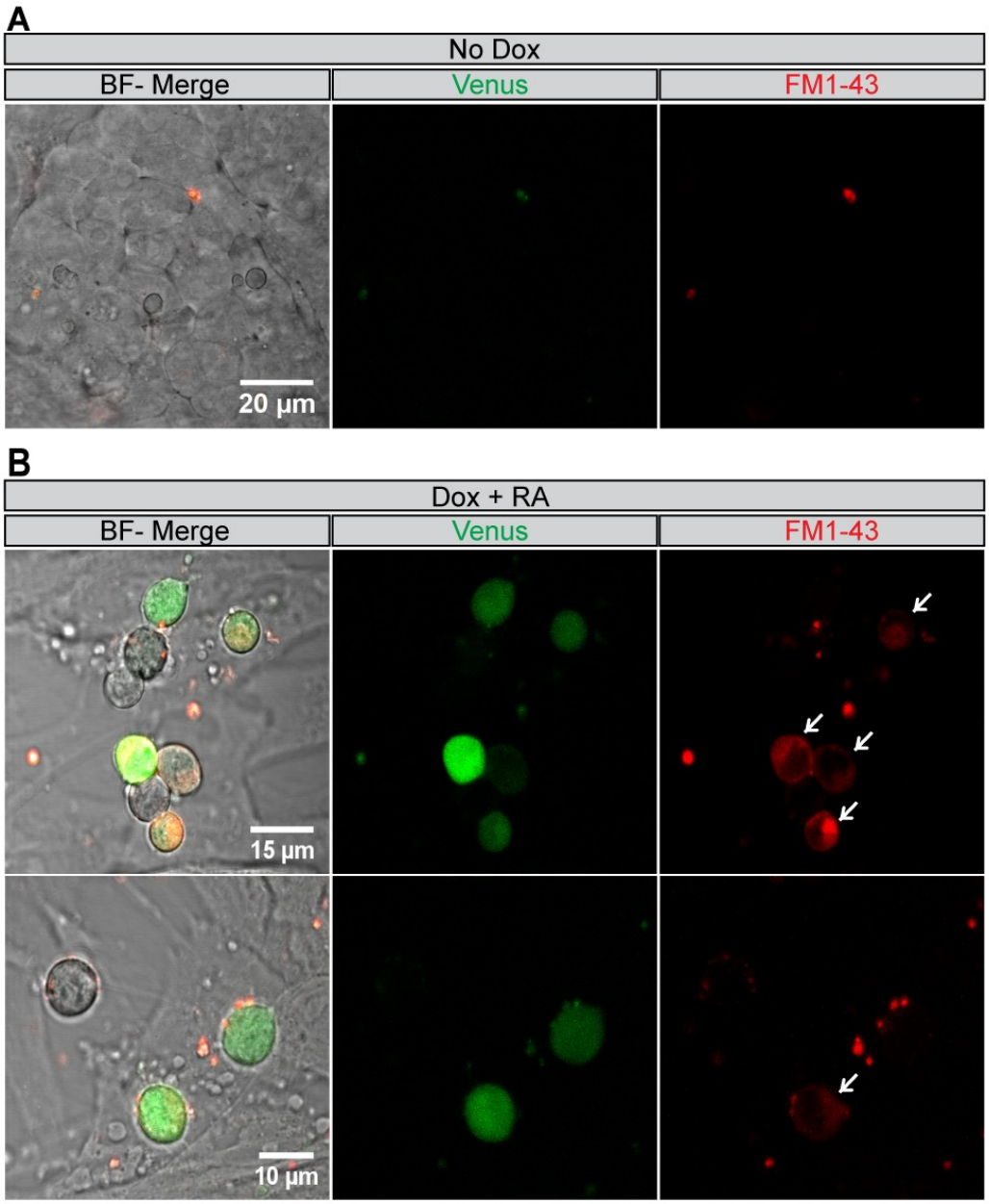

Fig. S7. iHCs express mechanotransduction channels that enable specific and fast FM1-43 permeation.

(A and B) The *in vitro* differentiation protocol (described in Figure 3E) for co-culture with embryonic chicken utricle mesenchymal cells was performed using the iGPA-Myo7a:mVenus reporter mESC line. At day 12, EB-derived cells grown in the presence or absence of Dox were incubated in 6µM FM1-43 for sixty seconds. Confocal bright field and fluorescence images in the "No Dox" condition shows absence of Venus and FM1-43 staining (A). In contrast, Dox treatment led to the appearance of Venus^{+} iHCs that are permeable to FM1-43 dye (arrows) (B).

BF, Bright field; FM1-43, N-(3-triethylammoniumpropyl)-4-(4-(dibutylamino)styryl) pyridiniumdibromide.

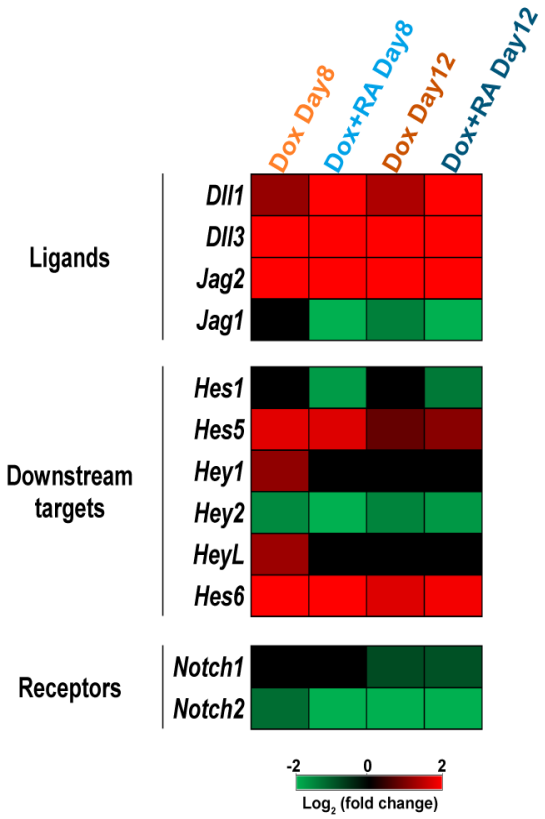

Fig. S8. The Notch pathway is active during iHC differentiation. Heat map depicting the relative fold changes in expression of various Notch pathway genes in the 4 iHCs populations at day 8 and at day 12. Only fold changes with a *P*<0,01 value are represented in this heat map.

Table S1. iHC transcriptome profile.

Worksheets: “Dox D8_UP-genes”, “Dox+RA D8_UP-genes”, “Dox D12_UP-genes” and “Dox+RA D12_UP-genes”. These contain all probe sets found to be significantly up-regulated (FC>2, *P*-value<0,01) in the four different iHCs groups, relative to uninduced cells.

Worksheets: “Dox D8_Down-genes”, Dox+RA D8_Down-genes”, “Dox D12_Down-genes” and “Dox+RA D12_Down-genes”. These contain all probe sets found to be significantly down-regulated (FC<-2, *P*-value<0,01) in the four different iHCs groups, relative to uninduced cells.

Worksheets: “D12>D8_Up-genes” and “RAD12>D8_Up-genes” contain all probe sets selected and analyzed by the criteria described in Figure 6F and G.

Worksheet “Deafness genes” contains a list of 88 genes and references used to generate the heat maps presented in Figure 6J and K.

Click here to Download Table S1

Table S2. Primary antibodies used for immunocytochemistry, immunohistochemistry and flow cytometry analysis.

Antibody	Species	Source & Catalog Number	Dilution
Myo7a	Mouse	Hybridoma Bank (DSHB), 138-1	1:100
Atoh1	Guinea-Pig	Kind gift of Y. Sasai lab	1:1000
Pou4f3	Rabbit	Sigma-Aldrich, HPA038215	1:50
Espin	Rabbit	Kind gift of A. J. Hudspeth lab	1:1000
Cdh23	Rabbit	Kind gift of Ulrich Mueller lab	1:200
Gfi1	Guinea-Pig	Kind gift of Hugo Bellen lab	1:2000
Myo6	Rabbit	Proteus Biosciences, 25-6791	1:800
Lhx3	Rabbit	Abcam, ab14555	1:200
Nestin	Mouse	BD Pharmingen, 556309	1:20
Sox2	Rabbit	Millipore, AB5603	1:200
Tuj1	Mouse	Covance, MMS-435P	1:500
GFP	Rabbit	Abcam, ab290	1:400
GFP	Chicken	Abcam, ab13970	1:1000
Parvalbumin	Mouse	Sigmag-Aldrich, P3088	1:200
HCS-1	Mouse	Hybridoma Bank (DSHB), (Hair Cell Soma-1)	1:100
HCA	Mouse	Kind gift of Guy Richardson	1:1000
3A10	Mouse	Hybridoma Bank (DSHB)	1:40
Prox1	Rabbit	Abcam, ab11941	1:200
E-cadherin	Mouse	BD Transduction, 610181	1:100
Cleaved Caspase-3	Rabbit	Cell signaling, 9661	1:200
Phalloidin-488	Probe conjugated to Alexa 488	Molecular Probes, A12379	1:100

Supplementary Material and Methods

Generation of iAtoh1 and iGPA ESC lines

Murine *Atoh1* ORF was amplified by PCR using the IMAGE clone IRAVp968D0993D as template. The PCR product was cloned into the Plox vector to produce the final Atoh1Plox vector that was used to generate the iAtoh1 mESC line. For the iGPA line, *Atoh1* ORF amplification was performed by adding a 2A peptide (2AP) sequence obtained from the *Thosea asigna* virus (TaV) of the *tetraviridae* virus family (Szymczak et al., 2004). This PCR product was cloned into the Plox plasmid, generating the 2APAtoh1Plox vector. Next, a similar 2AP sequence (designed from TaV) and the *Pou4f3* ORF were amplified from the IMAGE clone IRCKp5014M137Q and cloned into the 2APAtoh1Plox vector to produce the 2APPou4f32APAtoh1Plox vector. Finally, *Gfi1* ORF was amplified by PCR from the NM_010278 clone (kind gift from Dr. T. Möröy, University of Montreal) and cloned into the 2APPou4f32APAtoh1Plox vector to produce the final construct Gfi12APPou4f32APAtoh1Plox, herein named GPAPlox vector. To establish iAtoh1 and iGPA mESC lines, 20 µg of the respective Plox vector (Atoh1Plox and GPAPlox) and 20µg of a CRE expression plasmid (pTurbo-Cre) were electroporated into the Ainv15 ESC line (ATCC) (Kyba et al., 2002), and cells were selected using 350 µg/ml of G418,as previously described (Ting et al., 2005). Proper insertion of the Atoh1 and Gfi1-Pou4f3-Atoh1 cDNA was confirmed in G418-resistant colonies using PCR.

Generation of iGPA-Myo7a:mVenus ESC line

A regulatory DNA sequence of the murine Myo7a locus (including a 2063 bp DNA fragment from the 5' region upstream of the ATG initiation codon, and a 1776 bp fragment encompassing the Myo7a exon1 and intron1) was amplified by PCR using the BAC RP23-109F24 as template. This Myo7a regulatory DNA sequence (Boeda et al., 2001) was cloned into a vector containing the cDNA for mVenus and a poly(A) signal sequence followed by a selection cassette, which includes a phospho-glycero-kinase (PGK) promoter driving transcription of a Blasticidin resistance gene. The final Myo7a-mVenusPGKBlas vector was digested with Acc65I for linearization and electroporated into the iGPA mESC line. Electroporated mESCs were grown in the presence of 3 µg/ml blasticidin and resistant colonies (around 20 to 30 individual clones) were picked and expanded for further analysis. Differentiation assays were performed for each individual clone to evaluate the capacity to drive *mVenus* expression specifically in the iMyo7a^{+} population.

mESC cell maintenance and differentiation

All mESCs used in this study (Ainv15, iAtoh1, iGPA and iGPA-Myo7a:mVenus) were routinely grown at 37^{0}C in a 5% CO_2 incubator in *Dulbecco's* Modified Eagle's Medium (DMEM, Invitrogen), supplemented with 10% fetal bovine serum (FBS) (ES-qualified, Invitrogen), 2 ng/ml LIF and 1 mM 2-mercaptoethanol, on gelatin-coated (0.1%) Nunc dishes. Cells were passaged every other day, at constant plating density of 3×10^4 cells/cm^2.

For EB formation, mESCs were seeded on 60-mm bacterial-grade Petri dishes at 3×10^4 cells/cm^2, in DMEM medium in the absence of LIF. EBs formed within 24 hours, and medium was changed every 2 days. Supplementation with 2 µg/ml doxycycline (diluted in sterile PBS and filtered through a 0,2 µm filter unit) (Sigma-Aldrich), 1 µM retinoic acid (RA) (diluted in 0,01% DMSO) (Sigma-Aldrich) and 10 nM LY411575 (Lanz et al., 2004) (diluted in 0,01% DMSO) were initiated at day 4 and maintained until the required time point for analysis (day 8 or day 12). When required, 10 µM EdU (Molecular Probes) was added to cultures 30 min before fixation.

For co-cultures, 6 days old EBs untreated and treated with Dox + RA were dissociated using 0.25% trypsin-EDTA (Invitrogen) in PBS, and seeded (3.5x10^5 cells/cm^2) on top of inactivated embryonic chicken utricle periodic mesenchyme cells, in 4-well plates (Greiner). Co-cultures were grown using Dulbecco's modified Eagle's medium and Ham's F-12 (DMEM/F-12, Invitrogen) supplemented with 1x B27 and N2 (Invitrogen), in the presence or absence of 2 µg/ml Dox plus 1 µM RA. Medium was changed every 2 days until analysis at day 12. Isolation and inactivation by Mitomycin C (2 µg/ml, Sigma-Aldrich) of embryonic chicken utricle periodic mesenchyme cells (E17-18) was performed as previously described (Oshima et al., 2010).

Immunocytochemistry

EBs (6, 8 and 12 days old) were fixed with 1% paraformaldehyde (PFA) during 15 min at room temperature (RT). After fixation, EBs were cryoprotected in 15% sucrose (Sigma-Aldrich) in PBS, embedded in a solution containing 7.5% gelatine (Sigma-Aldrich) and 15% sucrose in PBS, frozen and cryosectioned (8-10 µm). EB sections were immersed in PBS at 37^{o}C until gelatin was completely dissolved, and then processed for immunocytochemistry. Fixed cells in coverslips or de-gelatinized EBs sections were blocked with 10% FBS and 0.05% Tween in PBS for 1 hour, followed by incubation overnight (O/N) with primary antibodies (Table S2). Sections were washed 3 times in PBS followed by incubation for 1 hour at RT with AlexaFluor-conjugated secondary antibodies (Molecular Probes) and 0.15% DAPI (Sigma-Aldrich). Detection of EdU incorporation was performed according to the manufacturer's instructions, Click-iT EdU Alexa Fluor 488 Flow Cytometry Assay Kit (Molecular Probes).

Electroporated embryos were fixed with 4% PFA at 4°C O/N, cryoprotected in 30% sucrose,embedded in 7.5% gelatin:15% sucrose in PBS, frozen, and 12 µm cryostat sections were prepared. Permeabilization was performed using 0.1% Triton X-100 for 10 min, followed by blocking (10% FBS, 0.1% Tween) for 1 h at RT. Primary antibodies were incubated O/N at 4°C (Table S2). Sections were subsequently washed and incubated with appropriate Alexa Fluor-conjugated secondary antibodies (Molecular Probes) for 1 h and 0.15% DAPI.

Imaging and cell counts

Fluorescent and bright-field images of fixed sections and cells were captured with DM5000B microscope using a DC350F camera (Leica Wetzlar, Germany), or using Zeiss LSM510 META, Zeiss LSM 710 confocal microscopes. Living cells and EBs were photographed under an upright 2-photon Zeiss LSM 510 META, and an inverted microscope Leica DMIL with a DC200 camera. All digital images were formatted with Photoshop CS (Adobe, San Jose, CA) and ImageJ.

The number of Myo7a, Espin, Pou4f3 and Venus expressing cells was quantified as a proportion of total number of induced cells (eGFP/Venus$^+$, Atoh1$^+$ or 3 TF$^+$ cells), or total number of cells in EBs (Dapi). The number of positively labeled cells was quantified by counting 4 to 5 randomly selected fields corresponding to a minimum of 10,000 cells, counted as DAPI nuclei. Three independent experiments were counted per each condition using Photoshop CS Cell Counter software.

Flow cytometry analysis

For live cell analysis, EBs were dissociated and resuspended in 4% FBS in PBS. All cells were analyzed in LSR Fortessa *(*BD Biosciences). For intracellular staining, fixed cells (15 min, 1% PFA) were blocked and permeabilized for 1 hour with 0.25% saponin and 5% sheep serum in PBS, followed by incubation for 1 hour with primary antibodies for Myo7a and GFP (Table S2). Cells were washed 2 times in 0.25% saponin in PBS followed by incubation for 1 hour with AlexaFluor-conjugated secondary antibodies (Molecular Probes). Data were analyzed with FlowJo software (Tree Star).

Scanning electron microscopy

The co-cultures of EB-derived progenitors and mitotically inactivated chicken utricle mesenchyme treated with Dox + RA were fixed with 2.5% glutaraldehyde in 0.1 M cacodylate buffer pH 7.3, with 3 mM $CaCl_2$, for 90 minutes at RT. After rinsing in buffer, cells were post-fixed in 1% OsO_4 in 0.1 M cacodylate buffer for 90 min. Samples were processed through the thiocarbohydrazide-OsO_4 repeated procedure (Davies and Forge, 1987) before dehydration in an ethanol series and critical point drying. Samples were mounted on scanning electron microscope stub and sputter-coated with

platinum. The cells were visualized in a JEOL 6700F cold field emission instrument operating (JEOL UK, Welwyn Garden City) operating at 3 or 5 kV.

FM1-43 uptake assay

Stock solutions of 3 mM FM1-43 [*N*-(3-Triethylammoniumpropyl)-4-(4-(Dibutylamino) Styryl) Pyridinium Dibromide) (Molecular Probes) were dissolved in water. To assess iHC fast permeation to the FM1-43 dye, co-cultures of inactivated utricle mesenchyme and iGPA-Myo7a:mVenus-derived progenitors, untreated or treated with Dox + RA for 8 days, were washed twice with Hanks' Balanced salt solution (HBSS, Invitrogen) and exposed for 60 seconds to HBSS solution containing 6µM of FM1-43. Live cells were immediately washed three times in HBSS solution and observed on an upright confocal microscope (Zeiss LSM 510 Meta) using a 40X water immersion lens. Several images were captured from live cultures in random fields immediately after dye application.

Real-time quantitative PCR

Real-Time quantitative PCRs were carried out using iTaq Universal Sybr Green Supermix (Bio-Rad) on 7500 Real-Time and ViiA 7 Real-Time PCR systems (Applied Biosystems). Primers were designed using Primer3 program followed by BLAST searches to confirm their specificity. All quantitative PCR data were performed with at least 2 repeats. The PCR products were confirm by proper melting curves and agarose-gel electrophoresis. The relative amount of each transcript was normalized to the level of GAPDH. Relative expression levels in the various Dox-treated samples were referred to the levels of expression in control untreated (without Dox) which were arbitrarily set to 1. The primer pairs sequences (forward and reverse) used: Myo7a (5'-AATCACATCAGGTACAGCGAAGA-3', 5'-CGGGGAAGTAGACCTTGTGGA-3'), Cdh23 (5'-AACAGCACAGGCGTGGTGA-3', 5'-TGGCTGTGACTTGAAGGACTG-3'), Espin (5'-GGTCTCAGCCACTGCTCAATG-3', 5'-GAATGTCTCGTCTCCAGGCAG-3'), Lhx3 (5'-AACAACAGTAACGCCTTGCTT-3', 5'-CACACGGCATTCCAGAACAG-3'), Myo6 (5'-GAGAGGCGGATGAAACTTGAGA-3', 5'-CTTCGGAGTGCCATGTCACC-3'), Atoh1 (5'-ATGCACGGGCTGAACCA-3', 5'-TCGTTGTTGAAGGACGGGATA-3'), Pou4f3 (5'-GCAAGAACCCAAATTCTCCA-3', 5'-TAGATGATGCGGGTGGATCT-3'), Gfi1 (5'-AGGAACGCAGCTTTGACTGT-3', 5'-TGAGATCCACCTTCCTCTGG-3'), Sox2 (5'-ATGGACAGCTACGCGCAC-3', 5'-CGAGCCGTTCATGTAGGTCTG-3'), Nestin (5'-CTGGAACAGAGATTGGAAGGCCGCT-3', 5'-GGATCCTGTGTCTTCAGAAAGGCTGTCAC-3'), Tuj1 (5'-AAGGTAGCCGTGTGTGACATC-3', 5'-ACCAGGTCATTCATGTTGCTC-3'), GAPDH (5'-ATTCAACGGCACAGTCAAGG-3', 5'-TGGATGCAGGGATGATGTTC-3').

Microarray sample preparation and data analysis

Total RNA was extracted from untreated EBs at day 8 and day 12, and from FACS-sorted EBs at day 8 and 12 treated with Dox or Dox + RA. All cells were derived from the iGPA-Myo7a:mVenus ES line. Cell sorting of Venus^{+} populations were done on a FACS Aria cell sorter (Becton Dickinson). RNA concentration and purity was determined by spectrophotometry and integrity was confirmed using an Agilent 2100 Bioanalyzer with a RNA 6000 Nano Assay (Agilent Technologies, Palo Alto, CA). RNA was processed for use on Affymetrix (Santa Clara, CA, USA) Mouse Genome 2.1 ST Arrays Strip by using the Ambion WT Expression Kit (Life Technologies, CA, USA) and Affymetrix GeneChip WT Terminal Labeling Kit, according to the manufacturer's protocols. Briefly, 100 ng of total RNA containing spiked in Poly-A RNA controls (GeneChip Expression GeneChip Eukaryotic Poly-A RNA Control Kit, Affymetrix) was used in a reverse transcription reaction (Ambion WT Expression Kit) to generate first-strand cDNA. After second-strand synthesis, double-stranded cDNA was used in an *in vitro* transcription (IVT) reaction to generate cRNA (Ambion WT Expression Kit). 15 µg of this cRNA was used for a second cycle of first-strand cDNA synthesis (Ambion WT Expression Kit). 5.5 µg of single stranded cDNA was fragmented and end-labeled (GeneChip WT Terminal Labeling Kit, Affymetrix). Size distribution of the fragmented and end-labeled cDNA, respectively, was assessed using an Agilent 2100 Bioanalyzer with a RNA 6000 Nano Assay. 3.5 µg of end-labeled, fragmented cDNA was used in a 150 µl hybridization cocktail containing added hybridization controls (GeneAtlas Hybridization, Wash, and Stain Kit for WT Array Strips, Affymetrix), of which 120 µl were hybridized on array strips for 20 h at 48°C. Standard post hybridization wash and double-stain protocols (GeneAtlas Hybridization, Wash, and Stain Kit for WT Array Strips, Affymetrix) were used on an GeneAtlas system (Affymetrix), followed by scanning of the array strips.

The 16 scanned arrays were analyzed first with Expression Console software (Affymetrix) using RMA to obtain expression values and for quality control. Control probe sets were removed and log2 expression values of the remaining 33710 transcripts were imported into Chipster 2.4 (Kallio et al., 2011). Differential expression was determined by empirical Bayes two-group test (Smyth, 2004) with Benjamini-Hochberg multiple testing correction and a p-value cut-off of 0.01. Gene ontology (GO) analysis was performed by the DAVID functional annotation tool (http://david.abcc.ncifcrf.gov/).

Chicken embryo *in ovo* electroporations

Fertilized White Leghorn chicken (Gallus gallus) eggs were incubated at 38^{0}C and 30–80% humidity to HH12 stage (Hamburger and Hamilton, 1992). *In ovo* electroporation of the chicken otic cup was performed as described previously (Freeman et al., 2012). The vectors pCAGGS-T2TP (encodes a transposase controlled by a CAGGS promoter)

(Takahashi et al., 2008) and pT2K-CAGGS-rtTA-M2, (for constitutive expression of a tetracycline-on activator located between the left and right ends of *Tol2*) (Takahashi et al., 2008) were co-electroporated with either pT2K-TRE-B1-H2BeGFP (consists of a bidirectional tetracycline-responsive element (TRE) controlling transcription of both eGFP fused with histone 2B (H2B) and a empty transcriptional unit) (Takahashi et al., 2008) or pT2K-TRE-B1-H2BeGFP-GPA (herein named TRE:GPA-eGFP), which is a modified version of pT2K-TRE-B1-H2BeGFP in which the ORF of Gfi1-2AP-Pou4f3-2AP-Atoh1 was directionally cloned downstream of the empty transcriptional unit of the vector multiple cloning site. At HH24 embryos, doxycycline (30 µ g per embryo, Sigma-Aldrich) was administered *in ovo* and embryos were harvested 2 or 4 days later.

Supplementary References:

Boeda, B., Weil, D. and Petit, C. (2001). A specific promoter of the sensory cells of the inner ear defined by transgenesis. *Hum. Mol. Genet.* **10**, 1581-1589.

Davies, S. and Forge, A. (1987). Preparation of the mammalian organ of Corti for scanning electron microscopy. *J. Microsc.* **147**, 89-101.

Freeman, S., Chrysostomou, E., Kawakami, K., Takahashi, Y. and Daudet, N. (2012). Tol2-mediated gene transfer and in ovo electroporation of the otic placode: a powerful and versatile approach for investigating embryonic development and regeneration of the chicken inner ear. *Methods Mol. Biol.* **916**, 127-139.

Hamburger, V. and Hamilton, H. (1992). A series of normal stages in the development of the chick embryo. 1951. *Dev. Dyn.* **195**, 231–272.

Kallio, M. A., Tuimala, J. T., Hupponen, T., Klemela, P., Gentile, M., Scheinin, I., Koski, M., Kaki, J. and Korpelainen, E. I. (2011). Chipster: user-friendly analysis software for microarray and other high-throughput data. *BMC genomics* **12**, 507.

Kyba, M., Perlingeiro, R. C. and Daley, G. Q. (2002). HoxB4 confers definitive lymphoid-myeloid engraftment potential on embryonic stem cell and yolk sac hematopoietic progenitors. *Cell* **109**, 29-37.

Lanz, T. A., Hosley, J. D., Adams, W. J. and Merchant, K. M. (2004). Studies of Aβ Pharmacodynamics in the Brain, Cerebrospinal Fluid, and Plasma in Young (Plaque-Free) Tg2576 Mice Using the γ-Secretase Inhibitor N2-[(2S)-2-(3,5-Difluorophenyl)-2-hydroxyethanoyl]-N1-[(7S)-5-methyl-6-oxo-6,7-dihydro-5H-dibenzo[b,d]azepin-7-yl]-L-alaninamide (LY-411575). *J. Pharmacol. Exp. Ther.* **309**, 49-55.

Oshima, K., Shin, K., Diensthuber, M., Peng, A. W., Ricci, A. J. and Heller, S. (2010). Mechanosensitive hair cell-like cells from embryonic and induced pluripotent stem cells. *Cell* **141**, 704-716.

Smyth, G. K. (2004). Linear models and empirical bayes methods for assessing differential expression in microarray experiments. *Stat. Appl. Genet. Mol. Biol.* **3**, 1544-6115.

Szymczak, A. L., Workman, C. J., Wang, Y., Vignali, K. M., Dilioglou, S., Vanin, E. F. and Vignali, D. A. A. (2004). Correction of multi-gene deficiency in vivo using a single 'self-cleaving' 2A peptide–based retroviral vector. *Nat. Biotechnol.* **22**, 589-594.

Takahashi, Y., Watanabe, T., Nakagawa, S., Kawakami, K. and Sato, Y. (2008). Transposon-mediated stable integration and tetracycline-inducible expression of electroporated transgenes in chicken embryos. *Methods Cell Biol.* **87**, 271-280.

Ting, D. T., Kyba, M. and Daley, G. Q. (2005). Inducible transgene expression in mouse stem cells. *Methods Mol. Med.* **105**, 23-46.